Atomic Mass Measurements of Stable and Unstable Nuclides

A Thesis

Submitted to the Faculty of Graduate Studies

University of Manitoba

In partial fulfillment

of the requirements for the degree

Doctor of Philosophy

by

Gary Robert Dyck

Winnipeg, Manitoba, Canada

January, 1990

ISBN 0-315-63362-X

ATOMIC MASS MEASUREMENTS OF STABLE AND UNSTABLE NUCLIDES

BY

GARY ROBERT DYCK

A thesis submitted to the Faculty of Graduate Studies of
the University of Manitoba in partial fulfillment of the requirements
of the degree of

DOCTOR OF PHILOSOPHY

Acknowledgements

I wish to thank my supervisor, Dr R.C. Barber for his endless supply of guidance, wisdom and patience. The debt that a young graduate owes his supervisor is one that, I suppose, can only be repaid indirectly, and over many ensuing years.

I am also grateful to my many colleagues in the In the Mass Spectrometry Group. Dr H.E. Duckworth established the laboratory and developed a large portion of the field (and first observed the mass effect of nuclear shell structure) making my work possible. Dr K.S. Sharma has also provides me with guidance and a good part of my education. Dr R.J. Ellis has been both an inspiring colleague and good friend. Mr Clifford Lander, Mr Jon Hykawy and Mr Bernard Hall have all given to me a great amount of assistance, insight and friendship.

The other members of my committee, Dr K. Standing, Dr G. Clark and Dr W. Johnson also went to a great deal of effort on my behalf, between reading my thesis, preparing the necessary reports and participating in my oral exams.

I have also had the good fortune of working with the many dedicated scientists at Chalk River Nuclear Laboratories. Dr Erik Hagberg skillfully led me through the ropes of the mass measurement program there, as well as sitting on my examining committee. Dr John Hardy, Dr Vernon Koslowsky and Dr Hermann Schmeing were a part of all the work that I did at CRNL and were a great help to me at all times. Mr Mike Watson and Mr Wayne Perry did so much of the work for every experiment.

My parents constantly provided all the kind of support that only parents can. Without them, none of this would have been possible for me.

I must specially thank my wife, Susan. She suffered with me through the whole process and, I am sure, provided every bit as much of the effort as I did, and certainly all of my inspiration.

This work was funded through grants from the Natural Sciences and Engineering Council of Canada.

Table of Contents

1 Introduction 1

2 Context and Implications of the Experiments 4
2.1 History of the Neutrino Mass Question 4
2.2 Theoretical Basis 5
2.3 Decay Energies 5
2.4 Implications of a Finite Neutrino Mass 8
2.4.1 Grand Unification Theories 8
2.4.2 Cosmology 9
2.5 Experimental Status 11
2.6 Masses of Unstable Nuclides 11
2.6.1 Historical Summary 12
2.7 Figures for Chapter 2 14

3 Experiments at the University of Manitoba 16
3.1 Equipment 16
3.1.1 Description of the Manitoba II Mass Spectrometer 16
3.1.1.1 Ion Sources 18
3.1.1.2 Peak Matching 18
3.1.2 Switching Control 21
3.1.3 The Duoplasmatron Ion Source 23
3.1.3.1 Discharge Mechanism 23
3.1.3.2 Construction 24
3.2 Gd-Tb 25
3.2.1 Motivation 25
3.2.2 Experimental Details 26
3.2.3 Results 27
3.3 Xe-Te 29
3.3.1 Motivation 29
3.3.2 Experimental Details 32
3.3.3 Results 33
3.4 Figures for Chapter 3 36
3.5 Tables for Chapter 3 50

4 Experiments at Chalk River Nuclear Laboratories 58
4.1 Equipment 58
4.1.1 The Chalk River On-Line Isotope Separator 58
4.1.2 Data Acquisition 61
4.2 Indium Mass Measurements 63
4.2.1 Motivation 63
4.2.2 Experimental Details 64
4.2.3 Results 65
4.3 Figures for Chapter 4 67
4.4 Tables for Chapter 4 82

5 References 84

Table of Figures

Mass couplings of fermion fields 15
The Manitoba II Mass Spectrometer 37
The electron bombardment ion source 38
The data acquisition system 39
Schematic diagram of the Power Supply Board 40
Schematic diagram of the Switching Board 41
Schematic diagram of the Amplifier Board 42
The duoplasmatron ion source 43
Decay Scheme of 158Tb 44
Diagram of Gd - Tb input data 45
Pairing energy in even A nuclei 46
Two-neutrino and no-neutrino double beta decay 47
Diagram of Xe - Te input data 48
Results of the Xe - Te adjustment 49
The Chalk River ISOL 68
The Helium Jet ion source 69
The FEBIAD ion source 70
The Mass Measurement System 71
Timing Diagram for Mass Measurements 72
Odd-N and Even-N S2n Values 73
Gamma Ray Spectrum at Mass 103 74
Gamma Ray Spectrum at Mass 104 75
Gamma Ray Spectrum at Mass 105 76
Mass and Voltage Spectra 77
Mass and Voltage Spectra 78
Mass and Voltage Spectra 79
Results of the 104In Mass Measurements 80
S2n Values in the Vicinity of Z = 49 81

Table of Tables

Second Order Image Aberration Coefficients 51
New doublet spacings in the Gd - Tb region 52
Auxillary data for the adjustments 53
Input data and results of the Gd - Tb adjustment 54
New doublet spacings in the Xe - Te region 55
Previous mass spectrocopic data in Xe - Te region 56
Input data and results of the Xe - Te adjustment 57
Results of the 104In mass measurement 83

Abstract

This work describes three experiments in which precise atomic mass differences are determined by the technique of high resolution mass spectrometry.

The Manitoba II mass spectrometer has been used to measure precise differences, involving naturally occurring nuclides, in two distinct studies, both of which have implications for the current work related to the question of neutrino mass.

The first is a set of 6 doublet measurements in the Gd - Tb region, which show that the decay energy of 1220.64 ± 0.83 keV is insufficient to allow the K-capture decay of ^{158}Tb to the 1187 keV level of ^{158}Gd, which was proposed as a possible candidate for low energy β decay in which the effect of a ν mass would be clearly seen.

The second study is one in which 4 doublet spacings were determined in order to provide precise $Q_{2\beta}$ values for the decays of ^{130}Te and ^{128}Te, which have long been of interest because they represent similar decays where the Q-values are significantly different.

In a third experiment the Chalk River on-line isotope separator (ISOL) has been used to determine the masses of unstable nuclides. The tandem Van de Graaff accelerator was used to produce ^{105}In, ^{104}In and ^{103}In which were then studied with the ISOL. This represents only the second time that masses of nuclides far from stability, other than alkali metals, have been determined directly.

Introduction

1 Introduction

Mass spectroscopy is the technique by which ions are separated according to their masses. Since the early beginnings of this field an important application has been the precise determination of atomic masses [Du 86]. Its early successes were the discovery of the whole number rule for masses and the determination of the existence of isotopes amongst light stable elements. Early atomic mass measurements were used to derive the packing fraction (or binding energy per nucleon) curve, which showed iron to have the lowest packing fraction (or highest binding energy per nucleon) of any nuclide. As the precision of these measurements was improved the existence of nuclear shell structure, associated with magic numbers [Du 54], and subsequently of nuclear sub-shells (in isotopes of Mo [Bi 63]) was demonstrated. The mass effect associated with the onset of nuclear deformation [Ba 64] was shown in plots of the double neutron separation energies (S_{2n}).

There are many complementary techniques used in measuring atomic mass differences. N-gamma measurements are made by inducing the capture of a thermal neutron by a parent and then summing the energy of the photons given off by the daughter nucleus as it de-excites. These measurements have very high precision, i.e. 1 keV or better. The precision associated with mass spectroscopic measurements rivals that of the (n,γ) measurements. Moreover, mass spectroscopic data can provide both differences which connect distant regions of the mass table and direct comparisons with ions composed of ^{12}C and well known secondary standards. These mass spectroscopic data are responsible for the high precision of the absolute masses of virtually all of the stable nuclides. Decay energies can be used to establish the masses of unstable nuclides, providing that the decay schemes are well known. Most of the mass data for nuclides remote from the line of stability were obtained from this type of measurement. The precision achieved for the masses of such nuclides can approach that

obtained mass spectroscopically for nuclides near stability. Reaction Q-values are also used to measure atomic mass differences by studying the energetics of different nuclear reactions. These reactions, besides those already mentioned, consist primarily of (d,p), (p,α), (d,α), (p,n), (p,t), and (p,γ) reactions although more exotic reactions are ocasionally used. These measurements, generally, have a precision of several keV, somewhat poorer than mass spectroscopic measurements.

The mass spectroscopic data may be combined with the reaction and decay Q-value data and treated as a large set of linear equations. Since these equations over-determine the masses of most of the known nuclides the appropriate method of deriving a set of "best" values for the masses is a least-squares fit of the data [Me 72; Sh 77; Wa 85]. As an on-going project, mass measurements are continually being compiled and adjusted (with a least--squares adjustment) in the Atomic Mass Evaluation [Wa 85].

The mass spectrometry group at the University of Manitoba has been active in the precise determination of atomic masses for many years. The work at Manitoba began in 1965 with the construction of the Manitoba II mass spectrometer [Ba 71], and grew out of work previously done at McMaster University. Amongst other things, it was at McMaster (with the instrument later known as Manitoba I) that the mass effect associated with the onset of nuclear deformation was first observed in isotopes of Nd, Sm and Gd at N=88 [Ba 64].

Recent work with the Manitoba II spectrometer has been directed at specific problems, such as measurements related to the determination of an upper limit of the electron-neutrino mass. For example, a set of measurements was made in the Ge - Se region in order to determine, precisely, the decay energy of ^{76}Ge [El 85]. This value gives the energy with

which neutrinoless double beta decay could occur in ^{76}Ge. It is of immediate value to the groups attempting to observe the decay mode by direct detection in large hyper-pure germanium detectors.

This thesis reports three experiments. The first two are again motivated by the specific problem of setting an upper limit for the mass of the neutrino. The first of these is a set of measurements of mass differences in the region about ^{158}Tb designed to investigate the energy available for the decay of ^{158}Tb by electron capture. It has been suggested [Ra 83] that electron capture could take place to an excited state in ^{158}Gd and that the branching ratios could indicate a non-zero rest mass for the electron-neutrino. In the second experiment the $Q_{\beta\beta}$ for the double beta decays of ^{128}Te and ^{130}Te were determined. These values are important in attempts to observe such decays directly and thereby deduce limits for the electron-neutrino mass. A discussion of the relevance of these determinations to the question of the mass of the electron-neutrino is given.

Some significant improvements to the instrumentation of the Manitoba II mass spectrometer were made during the course of these experiments. Two of these developments are described in this thesis: the construction of an electronic amplifier and timing device, for the data acquisition system; and a duoplasmatron ion source.

The third experiment is a measurement of the mass differences ^{105}In - ^{104}In, ^{104}In - ^{103}In, and ^{105}In - ^{103}In. This experiment involves short-lived nuclides but is similar to the systematic studies undertaken in this laboratory amongst the stable isotopes in the upper region of the mass table. Until now, mass spectroscopic techniques have only been used to study mass differences of alkali metals (see section 2.6.1) and to Br and Ga [Sh 89], in previous work. The experimental work described here provides a more general approach and, accordingly, the techniques are described in some detail, as well as the results.

Context and Implications of the Experiments

2 Context and Implications of the Experiments

2.1 History of the Neutrino Mass Question

Wolfgang Pauli first postulated the existence of the neutrino in 1933 [Pa 33] to explain why electrons emitted by beta decay had a continuous energy spectrum, rather than a fixed energy. This particle was presumed to carry the missing energy in the decay. Enrico Fermi then incorporated this particle in his quantum mechanical description of beta decay theory [Fe 34]. Fermi realized that information about the mass of the neutrino could be derived from the shape of the electron energy spectrum but found no evidence for a nonzero neutrino mass.

Recently the question of a finite mass for the neutrino has become a very important and controversial one. A nonvanishing neutrino mass would have important implications in elementary particle theories (section 2.4.1) and in cosmology (section 2.4.2). Although there have been many types of experiments directed at the resolution of this question (see for example section 2.3), the result has been a decrease in the upper limit of the possible mass. No experiment has conclusively demonstrated a lower limit greater than zero. Current elementary particle theory introduces three distinct flavours of neutrinos, the electron-neutrino, the muon-neutrino and the tau-neutrino, for which the upper mass limits are:

$$M(\nu_e) < 30eV; \quad M(\nu_\mu) < 420keV; \quad M(\nu_\tau) < 250MeV$$

at about the 95% confidence level [Ro 88].

2.2 Theoretical Basis

In modern theories of elementary particles there is a distinction between two possible "types" of mass, the Dirac mass and the Majorana mass. This distinction arises from the mathematical description of the particle fields and of the particle masses being described as couplings between these fields.

A basis for the fermion fields can be made from four linearly independent spinor fields. Two of these fields can be related to the other two by charge conjugation. One possible basis for the description of a fermion field (ψ) would be ψ_L, ψ_R, $(\psi_L)^C$ and $(\psi_R)^C$, where $\psi^C = C(\overline{\psi})^T$ [Gr 86]. The masses of fermions are described as the coupling between right-handed and left-handed field components. This results in two possible coupling schemes: coupling between the unrelated right- and left-handed fields (ψ_R and ψ_L), which yields the Dirac mass term, and coupling between terms related to each other by charge conjugation (ψ_L and $(\psi_L)^C$, since $(\psi_L)^C = (\psi^C)_R$), which yields the Majorana mass term (see figure 2.1). Charge conservation forbids couplings of the latter type for charged spinor fields, which leaves the (uncharged) neutrino unique among elementary fermions in that it can posses the most general mass matrix consisting of both Dirac and Majorana terms.

2.3 Decay Energies

Perhaps the most straight forward way of looking for a neutrino mass is by studying the energetics of beta decays. In the beta decay process an unstable nucleus (A,Z) decays to a more stable (lighter) nucleus (A,Z+1 or A,Z-1) by the emission of an electron and an anti-neutrino, or a positron and a neutrino, viz.,

$$N(A,Z) \rightarrow N'(A, Z+1) + e^- + \bar{\nu} \ ;$$

$$N(A,Z) \rightarrow N'(A, Z-1) + e^+ + \nu \ .$$

Since electrons and neutrinos carry lepton number L = 1 and positrons and anti-neutrinos have L = -1 this process can be seen to conserve both baryon number (since A = A) and lepton number. Since, in positron emission, the emitted positron and an orbital electron are released, the atomic mass difference between the parent and daughter atom must exceed the masses of the two released particles (e^- and e^+), which total 1 022 keV. Electron capture, in which an orbital electron is captured by the nucleus which then emits a neutrino, is an alternate process to positron emission and requires only that $M_{parent} > M_{daughter}$, since no positron is created. These processes are mediated by the weak interaction and maximally violate parity and charge conjugation [Wu 57]. A detailed description of beta decay is given by de Shalit and Feshbach [Sh 74].

If we consider the case of β^--decay, conservation of energy tells us that the maximum energy available to the emitted electron (corresponding to a "zero energy" anti--neutrino) is:

$$Q_{\beta^-} = M(A,Z)c^2 - M(A,Z-1)c^2 - I - M(\bar{\nu}_e)$$

where M(A,Z) is the mass of the atom with nucleus N(A,Z), $M(\bar{\nu}_e)$ is the rest mass of the electron anti-neutrino and I is the difference in total atomic binding energy of the parent and daughter nuclide. If we can accurately measure the end point of the electron energy spectrum and the atomic mass difference between the parent and daughter nuclei it is possible to solve for the neutrino mass.

The most sensitive test of a neutrino mass from β-decay data is the shape of the end-point β energy spectrum. In fitting curves corresponding to different, possible neutrino masses the end-point energy, given by the mass difference of the parent and daughter nuclides, is a fitted parameter. Thus, a more accurate value for this mass difference will provide a more accurate value for a neutrino mass measurement.

The most favourable decay for this type of measurement is the β^- decay of ^3H to ^3He. The beta spectrum can be measured in beta spectrometers or in detectors implanted with tritium. The first measurement of the neutrino mass was made from the ^3H beta spectrum by Konopinski [Ko 47] who deduced a neutrino mass of between 11 and 17 keV. Curran et al. later derived an upper limit of 1 keV for the neutrino mass from the ^3H spectrum [Cu 49]. Modern limits are, conservatively, on the order of 30 eV. The atomic effects on the spectrum [Be 72], though probably not fully understood, should be one of the simplest cases and the mass difference is reasonably, though not sufficiently, well known [Sh 86].

An attempt was made to measure the atomic mass difference between ^3H and ^3He with the Manitoba II mass spectrometer. The stability of the magnetic analyzer proved insufficient at the the low fields required to measure such low masses and the ionization efficiency was inadequate for the quantities of tritium which would be reasonable for experimental and safety considerations. These obstacles were the motivation for the improvements which were made to the magnetic analyzer of the Manitoba II mass spectrometer and the construction of the duoplasmatron ion source (see section 3.1.3). Further work is being done so that a new and useful determination may be made for the atomic mass difference.

2.4 Implications of a Finite Neutrino Mass

2.4.1 Grand Unification Theories

A resolution of the debate over neutrino mass would prove to be a powerful test of the mathematical models currently under consideration as a basis for a Grand Unification Theory (GUT). The standard SU(5) model predicts that mass of the neutrino should be zero by ruling out both types of coupling. In minimal SU(5) the right-handed neutrino (ν_R) does not exist. This prohibits a Dirac mass coupling, while Majorana invariant couplings are not possible with the Higgs content of the minimal model. This model, however, has fallen into disfavour as it has many other failings, notably that it does not include, naturally, CP violation [Kl 85].

The natural extensions of the standard model tend to lead to a nonzero neutrino mass. An SU(5) model with enlarged particle content [Ze 80] can generate a finite neutrino mass. In SO(10) a massive neutrino is a natural consequence. Here the elementary fermions of one family are placed in a 16-dimensional spinor representation. This representation consists of the 5-dimensional and 10-dimensional representations of the SU(5) models and one additional neutral fermion, which can only be interpreted as the right-handed neutrino, ν_R. This suggests a Dirac mass for the neutrino that is comparable to the mass of the u-quark. Gell-Mann, Ramond and Slansky have shown [Ge 79] that this, large, Dirac mass combined with a much larger Majorana mass leads to one very light neutrino and one very massive neutrino by the following argument.

Let us assume that the right-handed Majorana term (m_R^M) is much larger than the Dirac term (m^D). For the single flavour case the neutrino mass matrix would be of the form:

$$\left(\bar{\nu}_L \overline{(\nu_R)^C}\right)\begin{pmatrix} 0 & m^D \\ m^D & m_R^M \end{pmatrix}\begin{pmatrix} (\nu_L)^C \\ \nu_R \end{pmatrix} \qquad m_R^M \gg m^D$$

Diagonalization yields one very light Majorana neutrino with:

$$m_1 \approx \frac{(m^D)^2}{m_R^M}$$

consisting mostly of ν_L and one very heavy neutrino with:

$$m_2 \approx m_R^M \quad .$$

Though this simple model has its weak points, it illustrates the mechanism for generating small neutrino masses by mixing large Dirac mass terms with even larger Majorana mass terms.

The question of the mass of the neutrino is obviously an important one to the current development of a Grand Unified Theory. Lower limits on the possible mass of the neutrino set more stringent constraints on the mathematical models used and the demonstration of a non-zero mass for the neutrino would represent a substantial step toward an understanding of the fundamental nature of matter.

2.4.2 Cosmology

Both the masses and mass distributions (as a function of radius) of many galaxies have been determined from their tangential velocities at different radii as indicated in spectroscopic studies. An indication of the amount of visible matter for which this

mass is responsible is given by the mass to luminosity ratio (M/L), which is the ratio of the amount of mass within a region divided by the luminosity of that region. In units of solar masses and luminosity, the M/L of the region around our sun is approximately 10.

Studies of spherical and spiral galaxies have shown that their mass densities remain relatively constant with radius, while the amount of visible matter decreases quickly at larger radii. This means that the percentage of non-luminous mass increases with distance from the galactic center [Fi 82]. Further, for a disk shaped spiral galaxy to be stable, this additional matter must have a spherical distribution about the core of the galaxy, leaving primarily the visible matter to form the spiral shape.

Large clusters of galaxies and super-clusters have also been examined. This takes into account any possible matter in large regions between galaxies. From these measurements the M/L ratio averages to about 250 [Fi 82], which is in agreement with the results of other techniques, indicating that the mass distribution between galaxies is relatively constant over very large distances.

This unseen mass may determine the eventual fate of our universe. If one assumes that the average M/L ratio of the universe is 250 (and that the Hubble constant is 90 km s^{-1} Mpc^{-1}) then we are within a factor of two, a value which is within the uncertainties, of having a closed universe that will eventually collapse back into itself.

There have been many speculations about the nature of the dark matter. Shifts in the distribution of main sequence stars, dwarf stars [Tu 82], neutron stars, black holes, interstellar gas and dust and even gravitinos [Si 82] have all been suggested as possible candidates for the missing mass. There are, however, serious objections to each of these possibilities [Fi 82; Me 81].

The most likely candidate for this unseen mass appears to be a massive neutrino. Since there are about a billion times as many neutrinos as all other particles in the universe put together, a very small mass would be sufficient to account for the missing matter. Schramm [Ov 80] has calculated that a mass of only 25 eV for the neutrino could not only more than account for the missing mass observed, but would also provide enough mass to close the universe. Wilczek [Wi 80] has shown that with a mass of 35 eV, neutrinos formed during the creation of the universe would have been sufficiently slowed (by gravitational forces) to form into loose clumps and almost perfectly account for the formation of the different types of galaxies and the massive halos observed to surround them.

2.5 Experimental Status

Many different experimental methods have been used to lower the upper limits on the neutrino mass [Ka 84; Ro 88]. In this work two experiments are reported which are of direct relevance to the use of branching ratios and double-beta decay rates in the search for tighter limits on the mass of the electron-neutrino. The details of these techniques are given in sections 3.2.1 and 3.3.1 respectively.

2.6 Masses of Unstable Nuclides

It is now possible to extend the region of measured masses far from the line of beta-stability. Measurement of the masses in this region is of fundamental importance in the understanding of the various nuclear mass formulae and the models on which they are based. Since the parameters for these formulae have been fitted to the existing data, they all predict, with some accuracy, the masses of the stable nuclides. As one compares

the predictions of these formulae far from the region of stability, however, the predicted masses can be seen to diverge quite rapidly. Mass measurements far from stability thus provide increasingly stringent tests of the various models.

Mass measurements far from stability also provide understanding of previously unexplored regions of the mass surface. This can be particularly important for models such as the Liran-Zeldes model [Li 76] which divide the mass surface into regions bounded by the nuclear "magic numbers". The coefficients of these models must be fitted in each region and many of these regions consist entirely of unstable nuclides. Exploration of the region of heavy sodium isotopes has shown that the N = 20 shell closure is replaced with a region of strong deformation [Th 75]. This effect had been totally unexpected.

2.6.1 Historical Summary

The measurement of the masses of nuclides removed from stability poses special problems. Since it is not possible to collect a large quantity of the nuclides in question, traditional mass spectrometric techniques are not appropriate. Reaction Q-value measurements of very high precision have been made of nuclei near the valley of stability, but such measurements are not readily applied to nuclides very far from stability. Many precise Q_α measurements have resulted in well known mass differences along a number of α decay chains in the high mass region of the mass surface, but several of these chains have no connection to stable nuclides. Thus, the masses of these nuclides are not related to the known nuclides [Wa 88]. Clearly, such measurements are limited to those nuclides which decay by α emission. Measurements of Q_β values allow the determination of many more unstable nuclides, but are

generally less precise and require a detailed knowledge of the decay scheme of the parent nuclide, a requirement that is frequently difficult to meet because several complex decay schemes are sometimes overlaid. This severely limits the generality and reliability of the technique.

Mass spectrometric techniques were first used to measure mass differences of unstable nuclides directly at CERN [Th 75; Ep 79]. In the first set of measurements the nuclides were produced, stopped and surface ionized in a target-ion source and then mass analyzed by a magnetic analyzer. This technique was used to make mass measurements of heavy isotopes of Li and Na [Th 75]. In the second experiment mass separated ions from the ISOLDE isotope separator were stopped and re-ionized in the surface ionization source of a commercial, double focusing mass spectrometer which provided a much higher resolving power ($R \approx 5000$). Mass measurements were made of both heavy and light isotopes of Rb and Cs [Ep 79]. Since these techniques require efficient surface ionization of the nuclide to be measured, they are limited to the alkali metals.

More recently, new types of instruments have been developed. Recoil spectrometers, which measure the masses of reaction products, have been built at LAMPF [Vi 86] and GANIL [Gi 87]. These instruments are producing measurements in the low mass region with precisions of up to 120 keV. At CERN a cyclotron resonance mass spectrometer, consisting of two penning traps, has been built to mass analyze the ISOLDE beam. It has just begun to provide extremely high precision measurements, but is limited, again, to isotopes of alkali metals which have sufficiently long half-lives.

2.7 Figures for Chapter 2

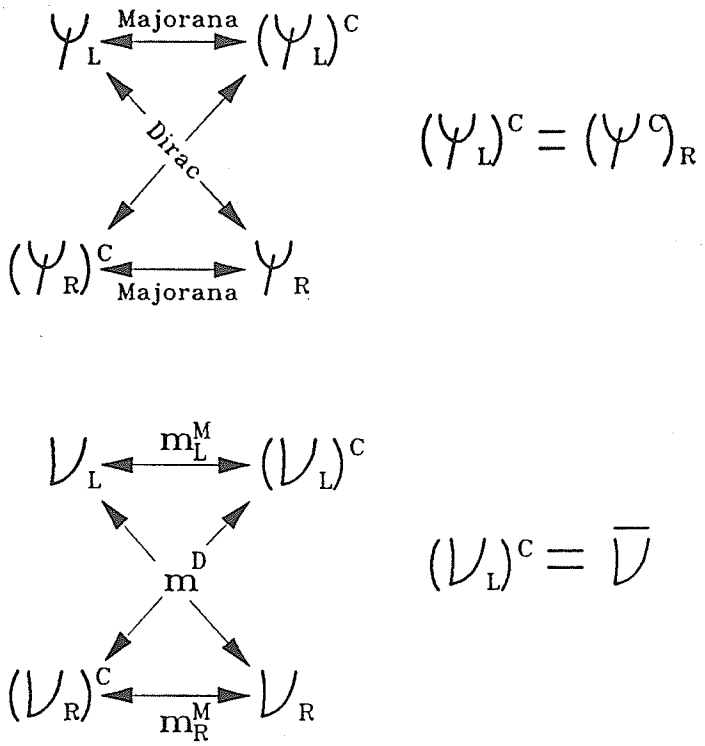

Figure 2.1 Mass couplings of fermion fields (from [Gr 86])

Experiments at the University of Manitoba

3 Experiments at the University of Manitoba

3.1 Equipment

3.1.1 Description of the Manitoba II Mass Spectrometer

The Manitoba II mass spectrometer (illustrated in figure 3.1) is a high resolution, double focusing instrument. The ion optical design of the instrument is one proposed by Hintenberger and König [Hi 59]. The instrument was designed to be double focusing (i.e. energy and direction focusing) to second order within a limited focusing theory which assumed abrupt boundaries to the electric and magnetic fields. Subsequent, detailed calculations, which take into account realistic fringe fields, showed that, although not zero, the important second order coefficients are certainly small (see table 3.1) [Ma 71]. The instrument may be operated with resolving powers (M/ΔM, where M is the nominal mass of the doublet and ΔM is the full width of the peak at 10% of peak height) in excess of 200 000.

Positively charged ions are formed in an ion source (as described in the next section) which is at a potential of approximately 19.4 kV. The extraction electrode is at ground potential. A set of vertical and horizontal steering plates, and an electrostatic quadrupole lens then position and focus the beam onto the principal slit, S_o, which has a width of 2.7 μm for a resolving power of 200 000. From this slit, the beam travels a distance l_e' before entering the electrostatic analyzer. In this drift region a second slit, S_α, with a typical width of 1.2 mm, limits the angular spread of the ions which enter the electrostatic analyzer to about $\pm 2 \times 10^{-3}$ radians.

A cylindrical electrostatic analyzer (ESA) then energy analyzes the beam. The ESA has a mean radius of 1 m with a 2 cm gap between the plates and subtends an angle of 94.65°. The ESA produces a direction focus with an energy dispersion at a distance l_e'' (= 17.63 cm) from its exit boundary. The energy defining slit, S_β has a typical width of 3 mm and limits the spread in velocities to about $\pm 8 \times 10^{-4}$. Between this slit and the magnetic analyzer is another drift space, l_m'. Immediately in front of the entrance to the magnetic analyzer is a height defining slit, S_h, which limits the height of the beam entering the magnetic analyzer (typically to 2.5 mm) and prevents the beam from scattering off of the top and bottom surfaces of the beam tube in the analyzer.

The magnetic analyzer is a 90° sector magnetic analyzer with a mean radius, r_m, of 62.74 cm and a gap width of 2.54 cm. For a singly charged ion at mass 300, the magnetic field is approximately 0.4 T. The homogeneity of the magnetic field was recently measured to be better than one part in 10^4.

The final focus of the machine is at the image slit, a distance l_m'' from the exit of the magnetic analyzer. In this region a pair of coils is used to sweep the ion beam across the detector slit (see section 3.1.1.2). Generally, a channeltron electron multiplier is used to detect all ions passing through the slit, although a set of channel plates was used for a large portion of the Gd - Tb measurements. The channel plates were found to give good, but inferior, gain and over all performance, with somewhat increased background noise.

3.1.1.1 Ion Sources

The ion source used for the Gd-Tb and Xe-Te measurements is similar to the Finkelstein ion source described by von Ardenne [Ar 62]. The particular design used by the group at the University of Manitoba, illustrated in figure 3.2, has been described in detail elsewhere [Bi 69; Me 71; Ba 71].

The sample is introduced into an oven in the center of the source. Gas samples may be leaked into the oven through a feedthrough and solid samples can be introduced either through a heated gas inlet or placed directly inside the oven. The oven has two holes along the axis of the source through which primary (ionizing) electrons enter the oven and positive ions are extracted. Directly behind the hole in the oven is a rhenium filament. The filament is heated by a current of about 13 A and thermionically emits an electron current of between 3 and 7 mA. The electrons are focussed and accelerated through the oven hole by a strong, axial magnetic field and an electric potential difference of approximately 135 volts between the filament and the oven. The electrons drift through the oven and then, on exiting through the other side, are repelled back into the oven primarily by the extraction field at the front plate of the source. The electrons oscillate through the oven and ionize the sample by electron bombardment. A plasma, sustained by continuous injection of electrons, is formed inside the oven and ions are extracted through the front hole.

3.1.1.2 Peak Matching

Doublet spacings were determined by the "visual null" method of peak matching (described in detail by Kozier et al. [Ko 79]). A peak is generated by

sweeping the ion beam across the collector slit by means of a sawtooth magnetic field and synchronously detecting the ion current that passes through the slit by a channel electron multiplier. The amplified ion current signal is displayed on an oscilloscope screen whose sweep is synchronized to the sweep of the sawtooth magnetic field.

A general theorem given by Swann [Sw 31] and later applied to mass spectrometers by Bleakney [Bl 36] shows that an ion of mass M′, initially at rest at a given location, will follow the same trajectory through the instrument as that of an ion of mass M, subject to the same initial conditions, provided that the magnetic fields remain constant and all of the applied electric potentials (V_i) are changed, so that

$$MV_i = M'V_i' \tag{3.1}$$

or

$$\frac{\Delta M}{M'} = \frac{\Delta V_i}{V_i} \tag{3.2}$$

where

$$\Delta M = M - M' \quad \text{and} \quad \Delta V_i = V_i' - V_i \tag{3.3}$$

The coincidence of these two ion paths is detected by observing the "visual null" signal which is derived in the following way. First the ion beam corresponding to mass M is swept across the collector with the potentials set to values V_i. For the next sweep all potentials are changed to values V_i' and the next mass peak M′ is detected. On alternate sweeps the normalized output from the detector is added or subtracted from the memory of a signal averager. This cycle is repeated for many sweeps (to improve the signal to noise ratio) and the signal representing the

difference between the peaks for M and for M′ is accumulated in the memory of the signal averager and displayed. The change in voltage for the electrostatic analyzer, $\Delta V_e = V_e - V_e'$ is then adjusted to find the matched condition where the two normalized peak signals cancel each other leaving a symmetric noise signal. The ratio $\Delta V_e/V_e$ is then measured with a precision voltage divider [Bi 70] and used in eqn. (3.2) to calculate the mass difference.

It should be noted that in a double focusing mass spectrometer the peak position is relatively insensitive to the other potentials applied to the instrument (e.g. those used to extract and form the ion beam before it enters the object slit). Consequently these potentials are set to their appropriate values for each of the masses, M and M′, at the beginning of a measurement and left unadjusted during the matching process.

There exists the possibility of a systematic error being introduced from the build up of a charged, insulating layer deposited on the surfaces of the electrodes. This means that the effective field seen by the ions is not directly determined by the potentials measured by the potentiometer. It has been shown [So 77] that this results in a systematic bias of the measured mass spacings that is proportional to the width of the doublet. A measurement is made of a well known, wide doublet (typically one or two mass units wide) to measure the size of the systematic bias. This correction is then applied proportionately to the measurement of the doublet in question. This error is typically on the order of 150 parts per million, a value which results in a correction of 0.15 μu for a doublet spacing of 1 000 μu. Typically this correction, for narrow doublets, is well within the statistical uncertainty associated with the measurements.

The data acquisition system used for this type of peak matching is illustrated in figure 3.3. A low thermal E.M.F. chopper generates the synchronizing signals for each sweep and applies the ΔV to the ESA plates. The switching unit determines the phase of the measurement cycle from the chopper signal and selects the gain of the normalizing amplifier and the voltages applied to the source, the quadrupole lens and the steering plates. It innitiates the required voltage changes at the end of a cycle, as indicated by the trailing edge of the oscilloscope sweep. This oscilloscope sweep signal is current-amplified and used to sweep the beam across the collector slit. Signals from the detector are routed through a pre-amplifier, an integrating amplifier, a normalizing amplifier and a summing amplifier (see section 3.1.2). The resulting signal is then presented to the signal averager, as described above.

3.1.2 Switching Control

The portion of the acquisition system which (a) separates and normalizes the two signals corresponding to M and M′ and (b) controls the timing of the voltage switching, is indicated in figure 3.3 by the dashed box. As a part of this work, this portion of the apparatus was re-designed to include active, operational amplifiers (instead of passive, resistive attenuators) to normalize the two peaks and mix signals, and solid state switches (instead of relays) to handle the switching of signals and voltages. The unit is composed of three printed circuit boards (a power supply board, a switching board and an amplifier board) inside a double width NIM module.

The power supply board (see figure 3.4) simply takes the +12V and -12V levels available from the NIM bin power supply and produces voltages of +5V, at up to

approximately 1A, and +2V and -2V at low current. A 7805 voltage regulator is used to regulate the 5V supply and the +2 and -2 V levels are regulated by three standard diodes in series, as these levels must be stable, although the actual value is not critical.

The switching board (figure 3.5) controls the timing of the voltages that are switched on the source, the quadrupole lens and the steering plates. The board senses the phase of the voltages that will be required from the A and $\overline{A}$ synchronization signals from the chopper and switches the voltages at the end of the previous sweep, so that they will settle during the time between sweeps. A differentiator (with voltage clamper for protection) detects the dropping edge of the oscilloscope sweep signal which marks the end of a sweep. The resulting pulse triggers a 555 timer, in a monostable configuration, which produces a clean TTL pulse. This pulse then serves as the clock pulse for a J-K flip-flop (5473). The phase of the output of the J-K is determined by the J and K inputs from A and $\overline{A}$ and is switched when a clock pulse is received. One of these outputs is then selected by a front panel switch to correspond to either an add or subtract measurement. The selected signal then powers a pair of solid state switches (half of a 4066) which, in turn, power a fiber optical switching system (also constructed during this work) for the source voltage and a relay for the quadrupole switching.

The amplifier board (figure 3.6) is built around a series of inverting amplifiers based on the 1458 dual operational amplifier. The first stage is an integrating amplifier which integrates the pulses from the detector. An adjustable offset voltage is available to cancel out any DC offset in the output. In the second stage the signal is split into two paths to go through two different (adjustable) gain resistors which are alternately selected, by solid state switches, to feed the amplifier on alternate sweeps. This

allows the amplifier to have a different gain on alternate sweeps so that the two peaks are normalized relative to each other. The choice of the resistors with respect to the phase of the switching is selectable by a front panel reversing switch. The maximum gain of this amplifier is limited by the on-state resistance of the switches of approximately 125 ohms. The third stage is capable of adding a small bias voltage to one of the two sweeps. This serves to split the two traces on an oscilloscope screen for focusing purposes. The final stage is a unity gain, inverting amplifier which inverts the signal to the proper polarity for the signal averager.

3.1.3 The Duoplasmatron Ion Source

The duoplasmatron is a development of the gas discharge ion source. In order to increase the efficiency of a gas discharge source one must increase the plasma density and the flux of hard electrons in the extraction volume [Si 78]. In the duoplasmatron there is a dual compression, first geometrically by the conical shape of the intermediate electrode and then magnetically by a strong axial magnetic field between the intermediate electrode and the anode [Le 74].

3.1.3.1 Discharge Mechanism

Electrons are emitted from the cathode and accelerated towards the intermediate electrode and anode, thus ionizing the gas and creating the plasma. The voltage between the cathode and the intermediate electrode shapes the plasma and forms a spherical double layer as well as a constriction of the plasma at the entrance to the intermediate electrode channel [De 62; Ki 65]. This double layer has a typical potential of 25V or more, converting many of the secondary electrons

into hard electrons. In some operating modes an additional double layer is formed within the channel. Another double layer is formed at the exit of the channel which again raises the electron temperature of the plasma. The second condensation of the plasma occurs between the intermediate electrode and the anode. The plasma is further heated by the remaining anode potential and concentrated by a strong axial magnetic field. The plasma extends through the anode into an expansion cup. An extraction electrode can then extract positive ions from this plasma with a strong electric field.

To extract negative ions from the source the electric field at the extraction electrode must be reversed. This would result in a prohibitively large electron current being extracted from the present geometry. This can be overcome by offsetting the axis of the cathode and intermediate electrode assembly from that of the anode [La 65; Co 65]. Provisions were designed into our ion source for extraction of negative ions by adjusting the displacement of these two axes with positioning screws. This method was used successfully in an ion source built by Aberth [Ab 67].

3.1.3.2 Construction

The duoplasmatron ion source was built as shown in figure 3.7. The magnetic return path (intermediate electrode, anode plate and return yoke) was initially constructed entirely of magnetic stainless steel, but the material was found to become porous on the anode plate after welding and hard soldering. This problem was overcome by constructing an anode plate from iron. Molybdenum inserts were used at the tip of the intermediate electrode and in the center of the

anode plate as these two locations are the most subject to sputtering by the plasma. Pains were also taken to get the water cooling as close as possible to these areas so that the life of the inserts might be extended. The magnet was wound on a copper spool which was nickel plated, to harden the o-ring surface, and water cooled. The cathode (or filament) was constructed of folded nickel mesh which was painted with an amyl acetate suspension of $BaCO_3$, $CaCO_3$ and $SrCO_3$ to increase the electron yield.

3.2 Gd-Tb

3.2.1 Motivation

A very sensitive way for detecting the mass of the neutrino is in the study of nuclear beta decays or orbital electron capture (EC) decays that have a very low decay energy. The case of EC decays is a particularly good one, in that there may be allowed decays involving the capture of orbital electrons from different shells. The existence of a finite mass for the electron neutrino would be reflected in the rates of EC to different final states. Since a neutrino mass would most strongly affect the rate of those decays with the least excess of energy, a measurement of the branching ratios would be a sensitive test for a neutrino mass.

The effect that a finite neutrino mass would have on the branching ratios of EC decay rates from different electronic shells would be on the order of:

$$[1 - m_\nu^2/(\Delta M - W_i)^2]^{1/2} \quad ,$$

where m_ν is the mass of the electron neutrino, ΔM is the atomic mass difference between the parent and the daughter atoms and W_i is the binding energy of the captured

electron in the daughter atom [Al 85]. This factor is caused by a phase-space deficit due to a finite neutrino mass [Ru 81]. It can be seen from the equation that the lower the excess energy (i.e. the denominator of the fraction) the larger the effect.

In 1983 Raghavan suggested that an observed, ultra-low energy K-capture branch in the decay from the ground state of ^{158}Tb to the 1187.13 keV state in ^{158}Gd (see figure 3.8) provided a favourable case for the determination of the electron--neutrino mass [Ra 83]. Other work ([Bu 84], [Al 85]), however, directed at establishing the energy difference between the ground states of ^{158}Tb and ^{158}Gd suggested that there might not be sufficient energy for this transition to take place, inasmuch as the required energy difference (Q_{EC}) would be the sum of the excitation energy and the energy associated with the K-shell in ^{158}Gd (50.24 keV), i.e., a required Q_{EC} > 1237.37 keV.

In order to derive an improved value for the mass difference ^{158}Tb-^{158}Gd, Burke [Bu 84] re-determined a precise value for the difference in Q-values for two (α,t) reactions and combined these with other, existing precise data, one of which was the spacing of a mass spectral doublet reported more than a decade ago by our group [Ba 72]. The important role of this doublet spacing in determining the decay energy, coupled with improvements made in our measuring techniques ([So 77],[Ko 80]), prompted us to re-examine that mass doublet and to determine a set of related mass differences [Dy 85].

3.2.2 Experimental Details

Accordingly, the spacings of six chloride doublets in the gadolinium - terbium region were determined, as given in table 3.2. The instrument was operated with a

typical resolving power of 160 000. The experimental techniques were those described in 3.1.1.2. The doublet spacings were measured with the "visual null" method of peak matching. Calibrations were made by measuring very wide doublets having spacings of two mass units, e.g. $^{157}Gd^{37}Cl^{35}Cl$ - $^{157}Gd^{35}Cl^{35}Cl$ = 1.997 049 890 u.

3.2.3 Results

The new data (table 3.2) are seen to be in excellent agreement with the 1983 atomic mass evaluation [Wa 85]. It should be noted that, while the mass evaluation includes all of our older mass spectroscopic values, it is completely independent of the values presented here. In a second, limited way, the reliability of the new data may also be assessed by their self-consistency. The loop formed by A-B-C (see figure 3.9) has the value 1.69 ± 2.09 μu, while the loop formed by D+E-F closes to within 0.20 ± 1.36 μu.

When the results are combined with the auxiliary data given in table 3.3, the doublet spacings may be expressed in terms of energy units and the neutron mass. These values are shown in table 3.4 together with the nuclear reaction and decay Q-values that are known in this region. As is evident from figure 3.9, these data over-determine the mass differences and, thus, the appropriate method for deriving a set of "best" values is through a least-squares evaluation of the data [Me 72; Sh 77]. The results of such an adjustment are summarized in the fifth column ("output") of table 3.4.

The output $Q_{EC}(^{158}Tb)$ value (code b_2, table 3.4) is 1220.64 ± 0.83 keV, a value that is clearly less than the 1237.37 keV required for the K-capture branch proposed

by Raghavan. Thus the electron-capture decay of ^{158}Tb to the 1187 keV level of ^{158}Gd is energetically forbidden. This value is higher than, but consistent with that reported by Altzitzoglou et al. [Al 85] by 4.2 ± 4.4 keV but clearly lower than that of von Dincklage [Di 85] by 12.4 ± 4.1 keV. It is in excellent agreement (1.3 ± 1.8) with the 1983 atomic mass evaluation.

Our work directly established the mass differences between the naturally occurring states in gadolinium and terbium with a precision of better than 1.1 keV. In particular, we have improved the precision of the important doublet D (see figure 3.9) by a factor of two. The reactions included in our least-squares calculation establish the position of the 180 year (ground) state in ^{158}Tb with a substantial improvement in the precision. The resulting data are: 1) self consistent, 2) consistent with previous data, and 3) result in a significant improvement in the precision to which the mass difference of ^{158}Gd and ^{158}Tb is known.

Altzitzoglou et al. studied the (p,d) reaction on a ^{158}Tb (180 a) target and concluded that the transition from that state does not allow sufficient energy for the decay proposed by Raghavan. A long lived isomeric state situated at least 16.7 keV above the 180 a state would allow the K-capture to take place as Raghavan suggests. Burke [Bu 84] has presented arguments against the existence of such a state. In the absence of any other evidence for its existence, we are forced to conclude that the K-capture of ^{158}Tb cannot proceed to the 1187 keV level of ^{158}Gd.

This work has been reported in Physics Letters 157B (1985) 139 [Dy 85].

3.3 Xe-Te

3.3.1 Motivation

Not all nuclei are able to decay toward a stable isobar by single beta decay, as described in section 2.3. An even-even nucleus is sometimes prevented from beta decaying towards the most stable (even-even) isobar by an intervening (odd-odd) nucleus which, because of the pairing interaction, is energetically inaccessible. For example, ^{130}Te cannot decay to ^{130}I since ^{130}I is more massive, even though ^{130}Xe is the lightest of the isobars (see figure 3.10).

These nuclei can decay only by double beta decay ($\beta\beta$ decay), in which two simultaneous beta decays occur so that the intermediate state is a virtual one, i.e.:

$$N(A,Z) \rightarrow N'(A, Z+2) + 2e^- + 2\bar{\nu} \ ;$$

$$N(A,Z) \rightarrow N'(A, Z-2) + 2e^+ + 2\nu \ .$$

This process can be seen to conserve lepton number.

At this point it is necessary to consider the difference between neutrinos and anti-neutrinos. Neutrinos were first detected by their ability to induce inverse beta decays. It soon became clear, however, that there were two different types of neutrinos. One type would induce inverse beta decays only in one direction, while the other would induce the opposite decay. If one type were considered a neutrino and the other an anti-neutrino and lepton number assignments were made as in section 2.3 then one could explain the properties of these neutrinos by proposing the law of conservation of lepton number. Studies of the angular momenta of weak interactions

showed that neutrinos had left-handed helicity, while anti-neutrinos had right-handed helicity. In fact, with no mass, charge or magnetic moment, this would be the only difference between them.

With a finite mass, however, the neutrino would be constrained to sub-luminal velocities. This would mean that for every left-handed neutrino there would be a frame of reference in which it would be right-handed or that the neutrino and anti--neutrino are the same particle. This would correspond to non-conservation of lepton number and should appear in the form of a neutrinoless double beta decay, since the nucleus could emit a neutrino and then re-absorb it as an anti-neutrino, inducing a second beta decay. The two decay modes are illustrated in figure 3.11 (after [Ha 82]).

Sophisticated new detectors are now able to look at the total energy carried off by the electrons in a $\beta\beta$ decay [Av 88]. This technique yielded the first direct observation of a $\beta\beta$ decay in 1987 [El 87]. As in the case of single β decay, the two-neutrino decay mode would produce a continuous spectrum of total electron energies. The no-neutrino mode, however, would produce a sharp peak at the end-point energy of the two-neutrino decay spectrum.

Since a no-neutrino $\beta\beta$ decay requires only two particles to be created, the resulting phase-space considerations would make half-lives characteristic of this mode shorter by an order of magnitude or more. Thus this should provide a very sensitive probe of neutrino mass, if sufficiently accurate half-life calculations and measurements are available.

Half-life calculations are only good within the accuracy of the nuclear--matrix-element calculations used. Comparison of these calculations with measured half-lives have shown that these calculations are not exceptionally reliable. It has

been suggested [Po 68] that the ratio of the double beta decay rates for ^{128}Te and ^{130}Te may reflect a violation of lepton number conservation and consequently yield limits for the mass of the electron-neutrino. Such calculations require a knowledge of the double beta decay lifetimes of ^{128,130}Te, the relevant matrix elements for these decays and the Q-values for each case. The lifetimes are obtained from various geochemical measurements on old tellurium ores. Considerable effort has also been spent on improving our understanding of the nuclear matrix elements [Do 81; Ha 82; Mi 83; Sc 85]. Finally, the analysis requires the use of a phase space factor that varies roughly as the ratio of the double-beta decay Q-values to the sixth power.

The half-lives of ^{128}Te and ^{130}Te, which decay to ^{128}Xe and ^{130}Xe respectively, can be measured in bodies of tellurium ore. Although the calculation of the half-lives and the half-life ratio depend strongly on the decay energy (or the mass difference), improved values for these mass differences do not provide new information regarding the nature of the decays. Instead, the improved information provides a precise value for the total energy available, so that searches for direct observations of the transitions may be made within narrow energy limits, as has been the case for ^{76}Ge [El 85; Av 88], by determining, unambiguously, the energy of any no-neutrino $\beta\beta$ decay. It is this latter consideration that has prompted the current work.

To this end, we have determined the mass differences for four mass spectral doublets involving isotopes of tellurium and xenon with the Manitoba II mass spectrometer [Dy 89].

3.3.2 Experimental Details

For this work the instrument was operated with resolving powers ranging from 100 000 to 180 000. The doublet spacings were determined by the "visual null" method of peak matching described in section 3.1.1.2 and by Kozier et al. [Ko 79].

The possible existence of systematic effects that could bias the mass determinations were meticulously examined and either eliminated or compensated for. In particular, the following effects were examined.

i) Systematic errors may be caused by the build up of charged layers on the surfaces of the electrostatic analyzer plates. Corrections were made for these by measuring calibration doublets as outlined in 3.1.2.

ii) Although the ion paths for M and M′ may be made to coincide at the collector slit (for the matched condition), they may fail to do so elsewhere unless all of the conditions of Bleakney's Theorem are satisfied. For example, if one of the two doublet members is formed with initial kinetic energy, while the other is not, they will in general follow slightly different ion paths through the spectrometer, even if the matched condition (eqn.2) is apparently satisfied, because the paths again coincide at the collector. Under such circumstances it is possible that the two ion beams could, on the average, experience slightly differing magnetic field strengths as a result of inhomogeneities in the applied fields and that systematic errors in the measured mass difference could result. To compensate for such differences in the initial kinetic energy of the ions, the value for the accelerating voltage $V_{a'}$ (for mass M′) is adjusted so that both ion groups are focused at the same point on the energy dispersive, focal plane of the electrostatic analyzer. This is done by displaying the matched peaks on

an oscilloscope and adjusting the value of ΔV_a until varying V_a results in both peaks being cut off simultaneously by the energy defining slit. This ensures that both of the ion groups have the same initial kinetic energy.

For the measurements presented here the Te^+ ions were formed from the fragmentation of the molecule $TeCl_5$, while the Xe^+ ions were formed by ionizing single atoms. As a result we observed that the Te^+ ions were often formed (depending on ion source operating conditions) with an additional kinetic energy relative to the Xe^+ ion. The energy resolution was better than 0.5 eV.

iii) It has been noted [Da 63] that the Te^+ mass spectra could become contaminated with ions from the mass spectra of doubly charged tellurium dimers, Te_2^{++}. This occurs when the ions are derived from a pure metallic sample. These species are characterized by a prominent peak at A = 129 and other peaks which are difficult to resolve from the single atom spectra. In particular, in this work $^{130}Te^{126}Te^{++}$ could be present as a peak that is not resolved from ^{128}Te at M = 128. To avoid this, the tellurium ions were produced by the fragmentation, under electron bombardment, of $TeCl_5$. Ions of the type Te_2^{++} were not observed at mass 129 thus assuring the absence of an unresolved Te_2^{++} contaminant at mass 128.

3.3.3 Results

The new data are presented in table 3.5. In every case they are seen to be in excellent agreement with the 1983 Atomic Mass Evaluation [Wa 85]. The region of the mass table under consideration includes previous mass spectroscopic work of our group and several others [Ba 64; Da 63; Ke 70; Ha 84] as listed in table 3.6 and

illustrated in figure 3.12. The new data are seen to be internally consistent in that, when combined with the absolute mass measurements of ^{130}Xe and ^{128}Xe, the loop formed by C-A-(r,s-t,u)+B closes to 0.07 ± 3.45 μu.

These new results represent a substantial improvement in precision over the corresponding values in the 1983 Atomic Mass Evaluation and are consistent with previously accepted data.

These data over-determine the desired energy differences and, accordingly, the appropriate method for deriving a set of "best" values is a least-squares evaluation of the data [Me 72; Sh 77]. Using the previous mass spectroscopic data, listed in table 3.6 and the auxiliary data of table 3.3, we have derived the input values in table 3.7. The results of such an adjustment are listed in the "Output" column of table 3.7.

The only previous measurement of the ^{126}Te^{35}Cl-^{124}Te^{37}Cl doublet was made by our group in 1963 at McMaster University with the 2.74m radius instrument (later "Manitoba I")[Ba 63]. This value is considerably lower than those of both our current work and the mass table. At the time, a considerable amount of data on this doublet had been rejected because of large, systematic shifts in its value. If all of the data are included, the result is a doublet spacing of 3438.7 ± 2.5 μu rather than the published 3432 ± 2 μu. This would put it in agreement with both our current value and that of the 1983 Mass Evaluation. Accordingly, this datum has been left out of the input data to the least-squares adjustment presented in this work and we recommend that our new value replace the old one.

The output values from table 3.7 yield a $Q_{2\beta}$ of 2 528.83 ± 1.34 keV for ^{130}Te and 867.27 ± 1.14 for ^{128}Te. These output values are compared with the mass dif-

ferences derived in the 1983 Atomic Mass Evaluation in figure 3.13. In all cases the addition of our new data improves the precision of the values for the mass differences in question.

The resulting improvement in precision of the Xe - Te mass differences by, typically, a factor of three is crucial in the search for the two modes of $\beta\beta$ decay. It is this energy value which would allow a no-neutrino $\beta\beta$ decay signal to be unambiguously distinguished from a two-neutrino $\beta\beta$ decay or some other decay signature.

3.4 Figures for Chapter 3

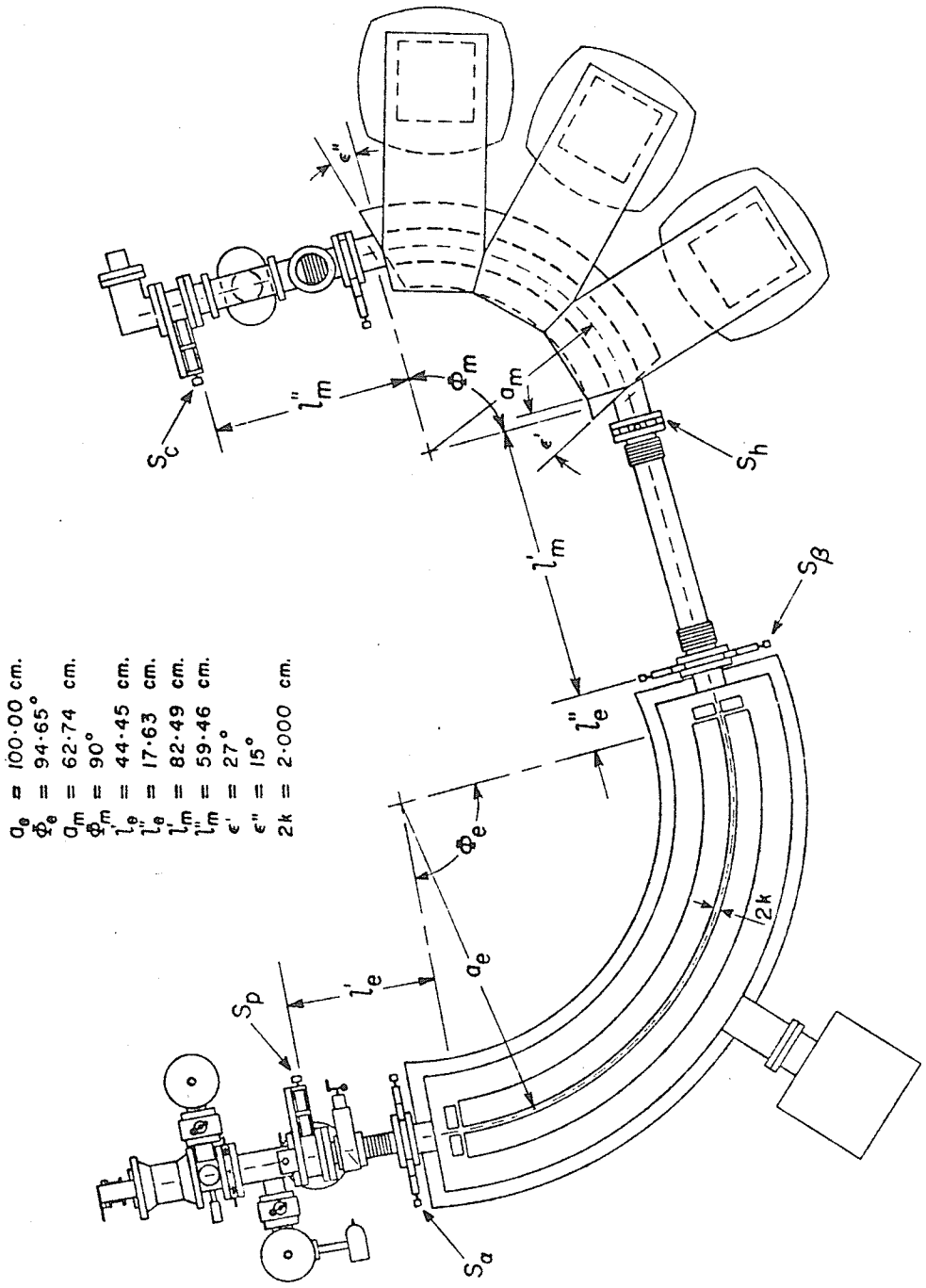

Figure 3.1 The Manitoba II Mass Spectrometer

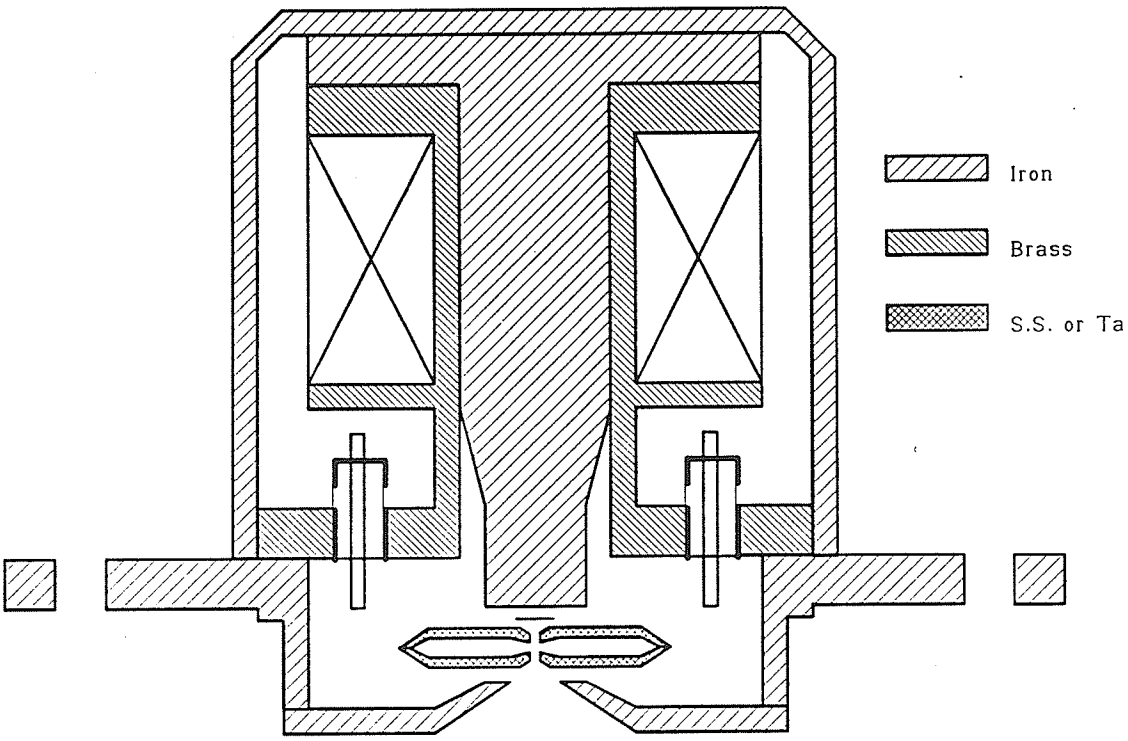

Figure 3.2 The electron bombardment ion source

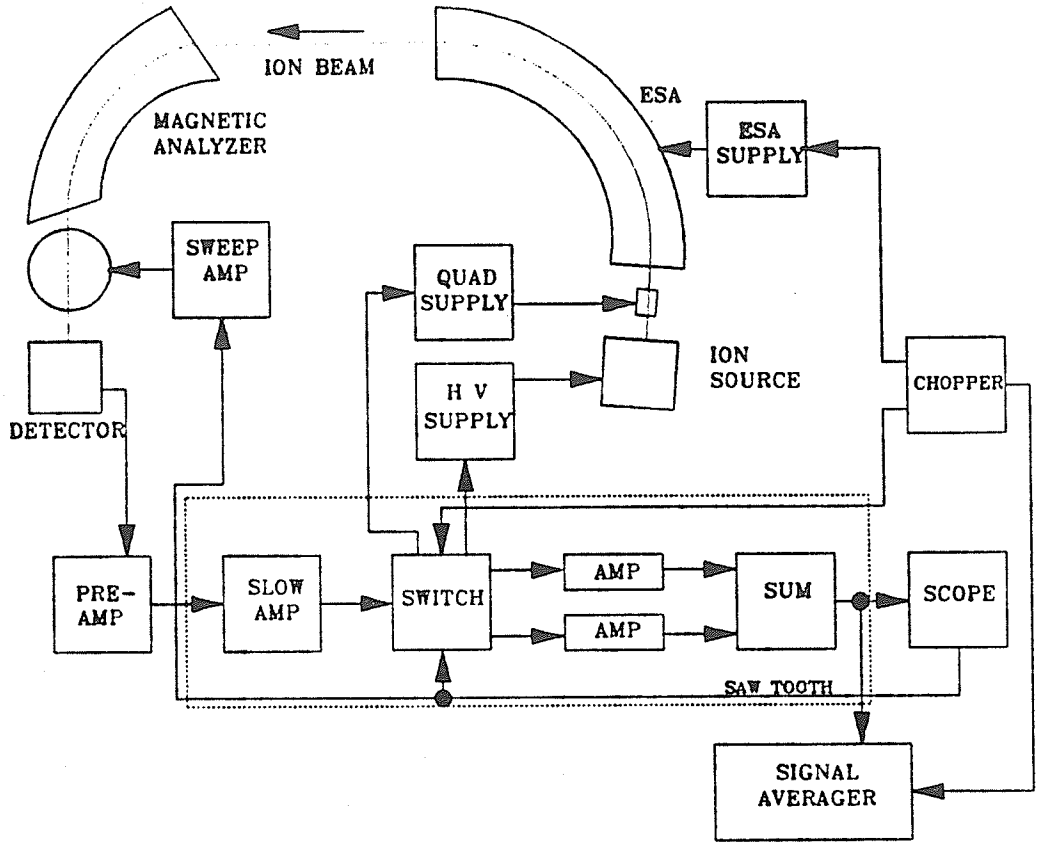

Figure 3.3 The data acquisition system

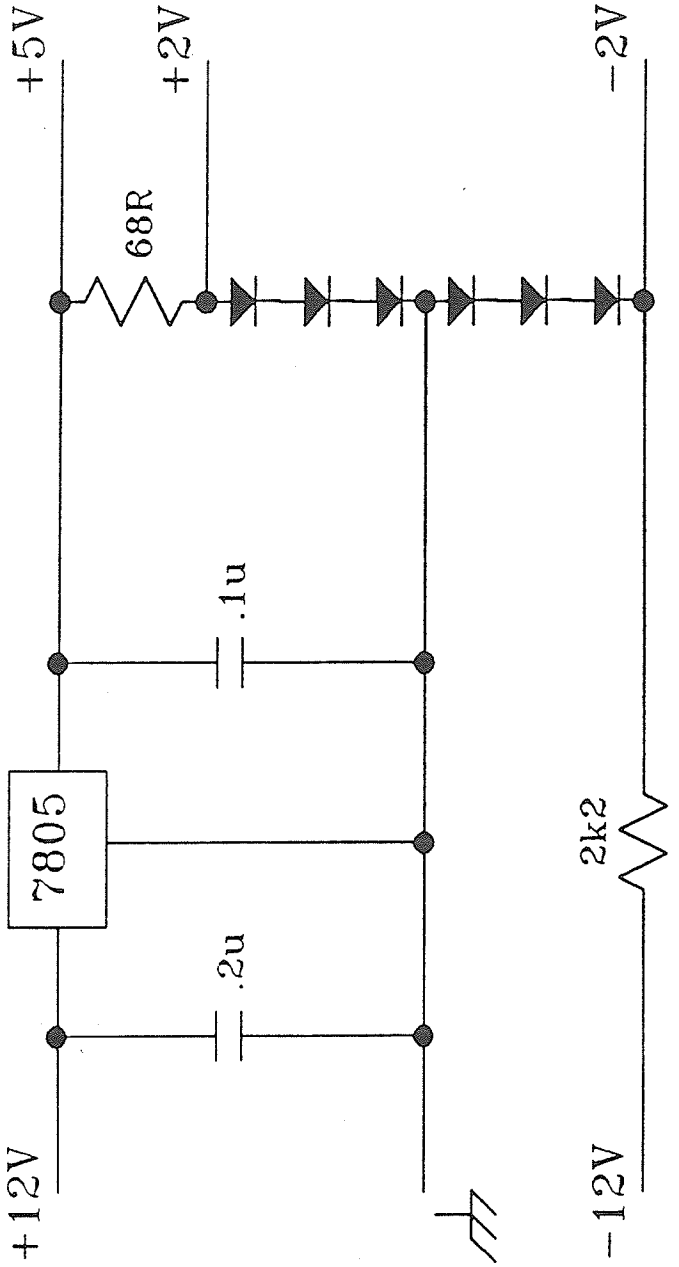

Figure 3.4 Schematic diagram of the Power Supply Board
All diodes are type 1N4005

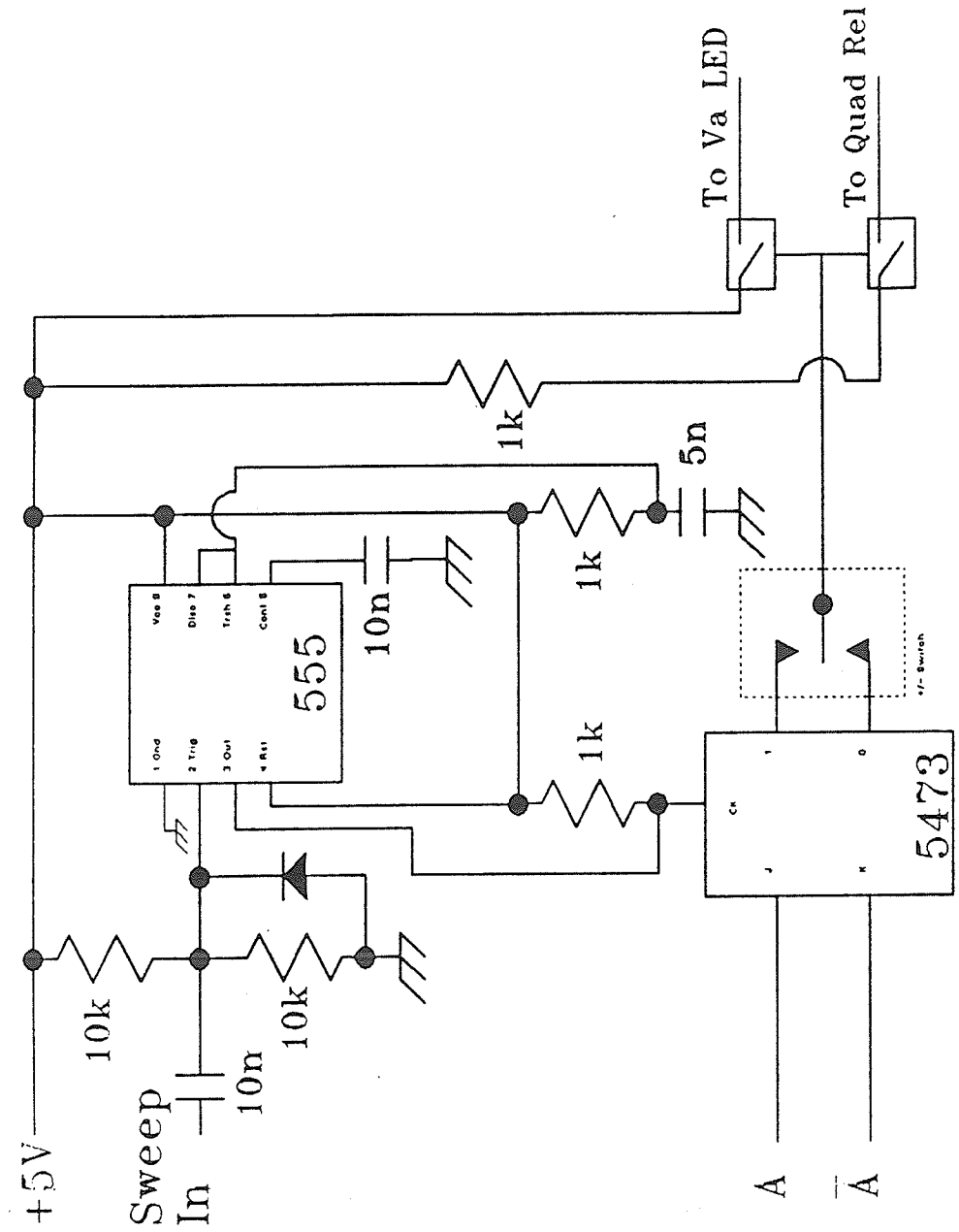

Figure 3.5 Schematic diagram of the Switching Board

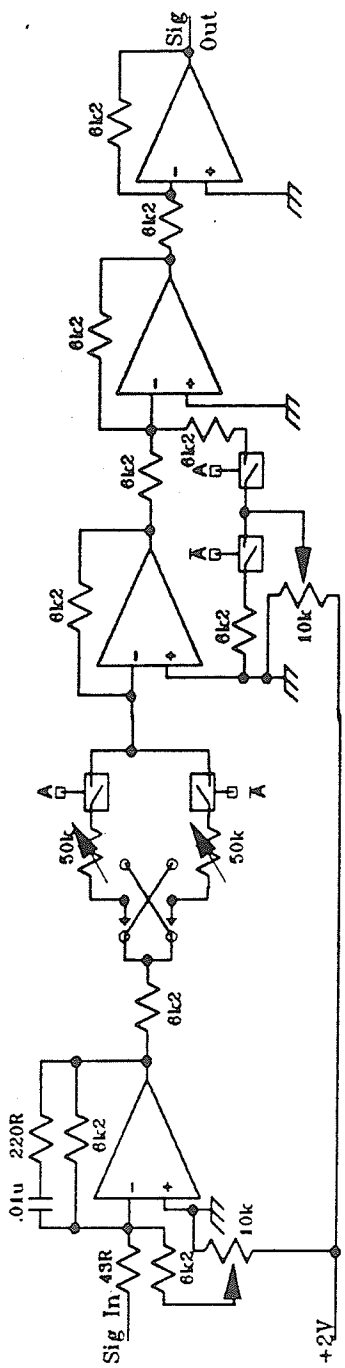

Figure 3.6 Schematic diagram of the Amplifier Board

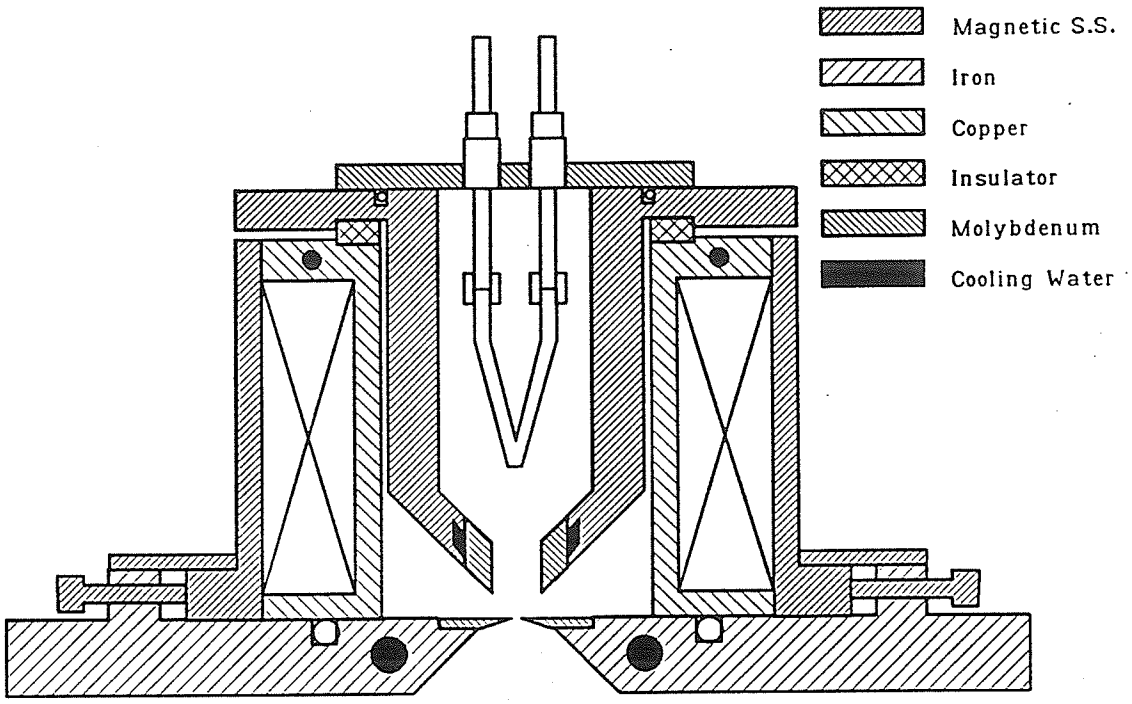

Figure 3.7 The duoplasmatron ion source

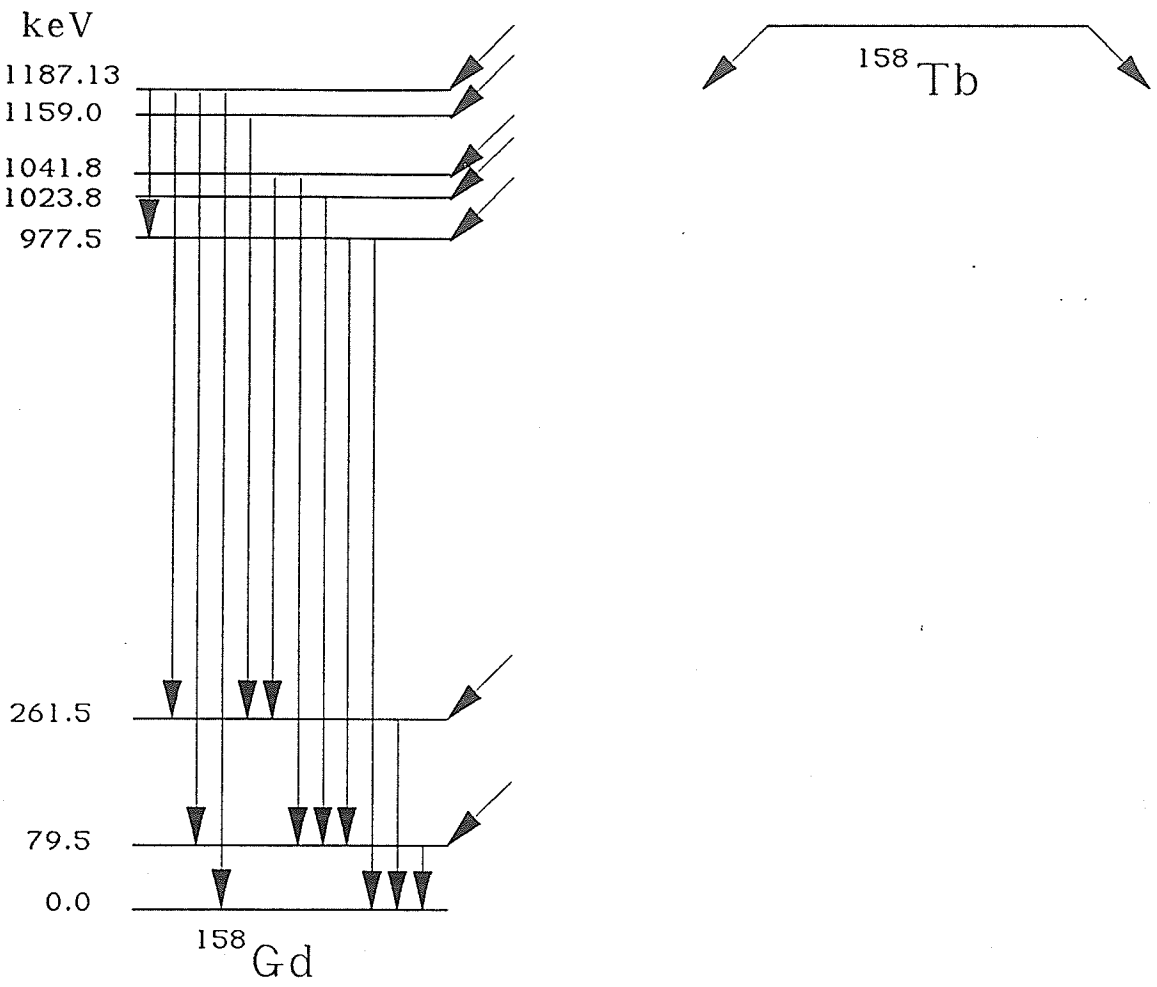

Figure 3.8 Decay Scheme of ^{158}Tb EC to ^{158}Gd

From the data of Tuli [Tu 74]

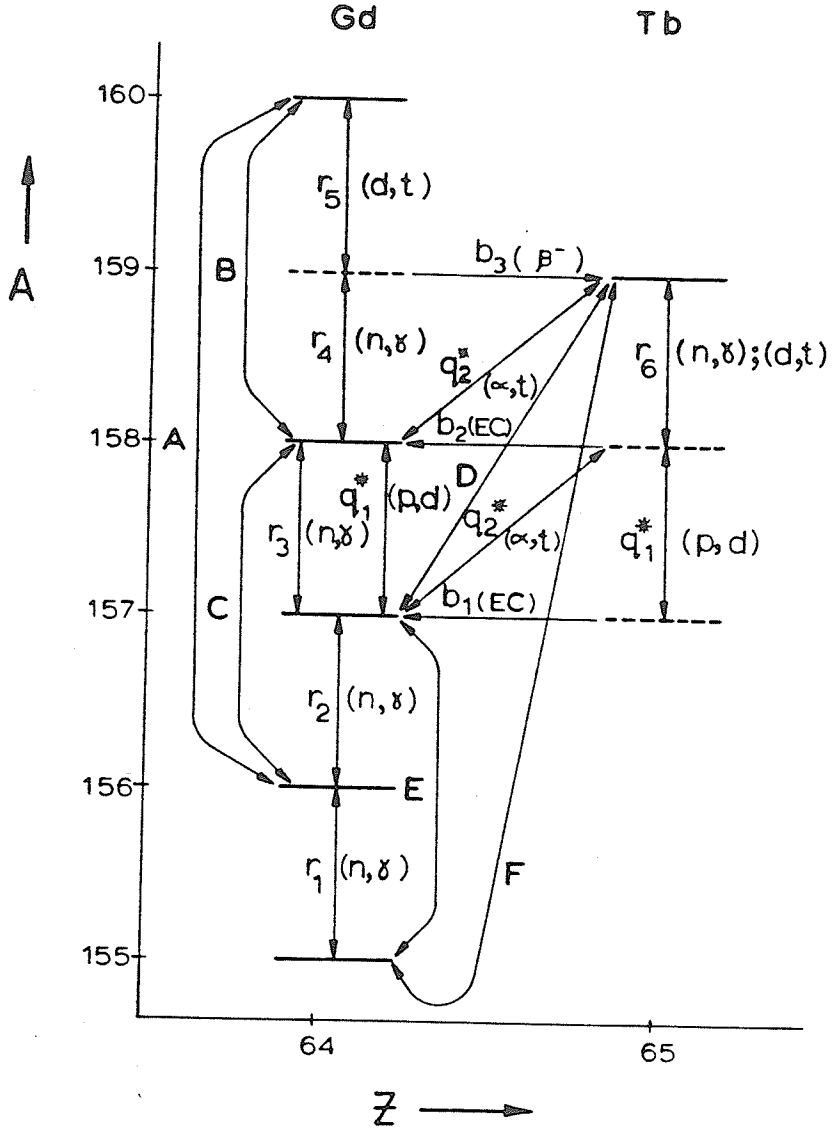

Figure 3.9 Schematic diagram of the Gd - Tb input data. From [Dy 85]

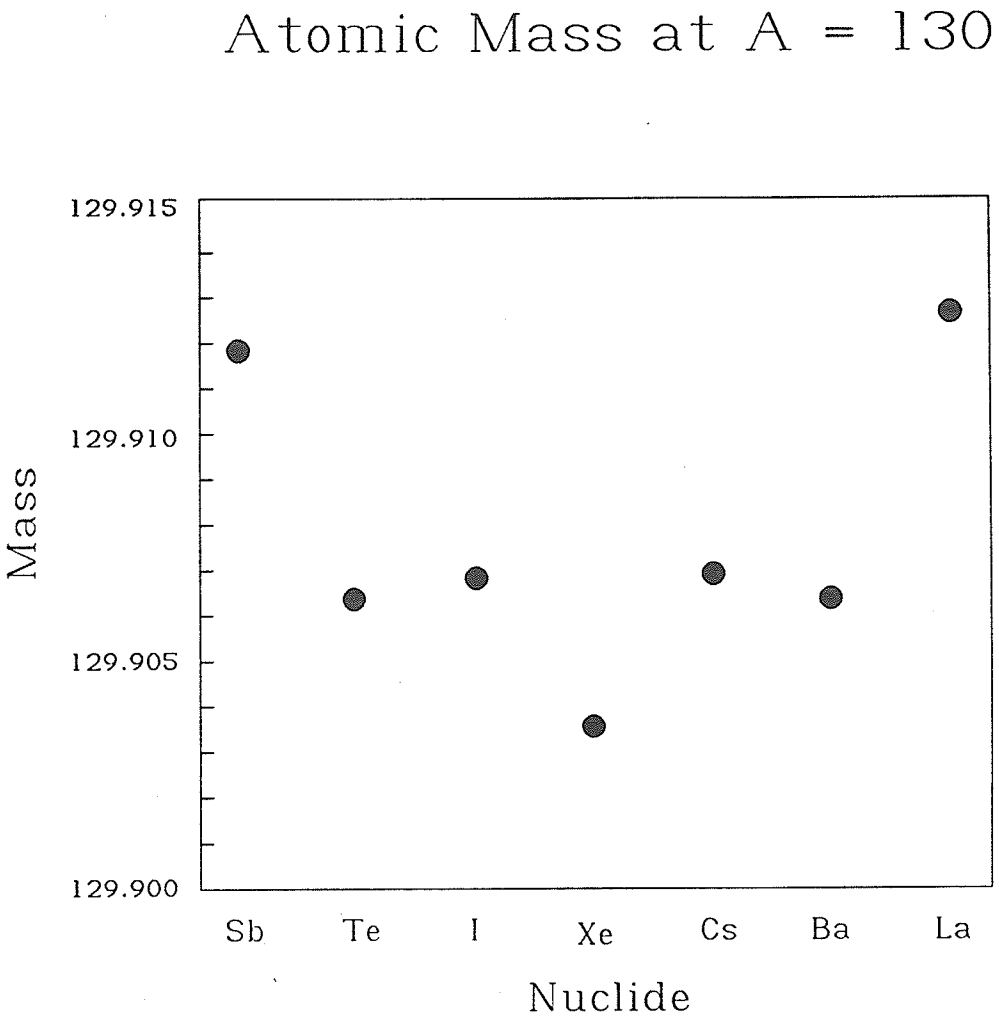

Figure 3.10 Effect of pairing energy on masses of even A nuclei

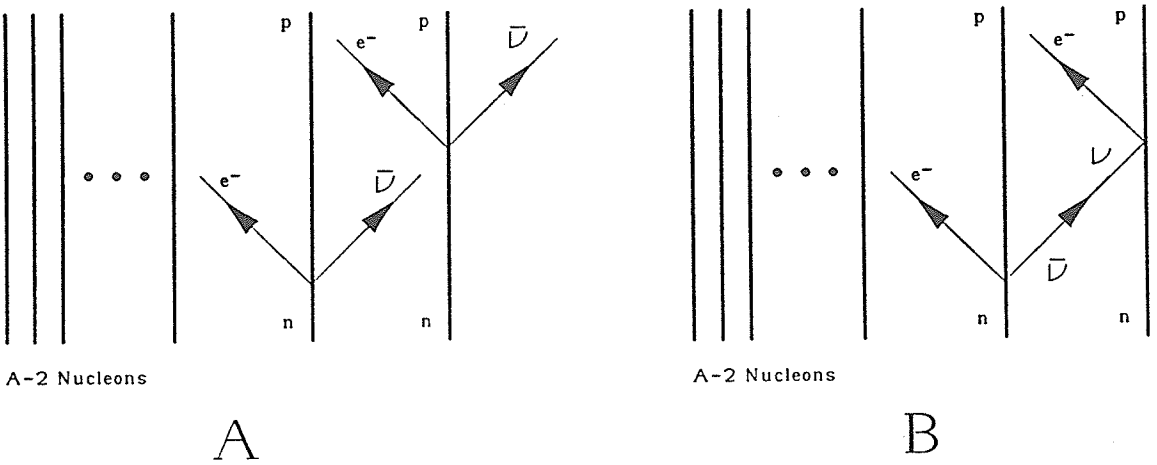

Figure 3.11 Two-neutrino and no-neutrino ββ decay

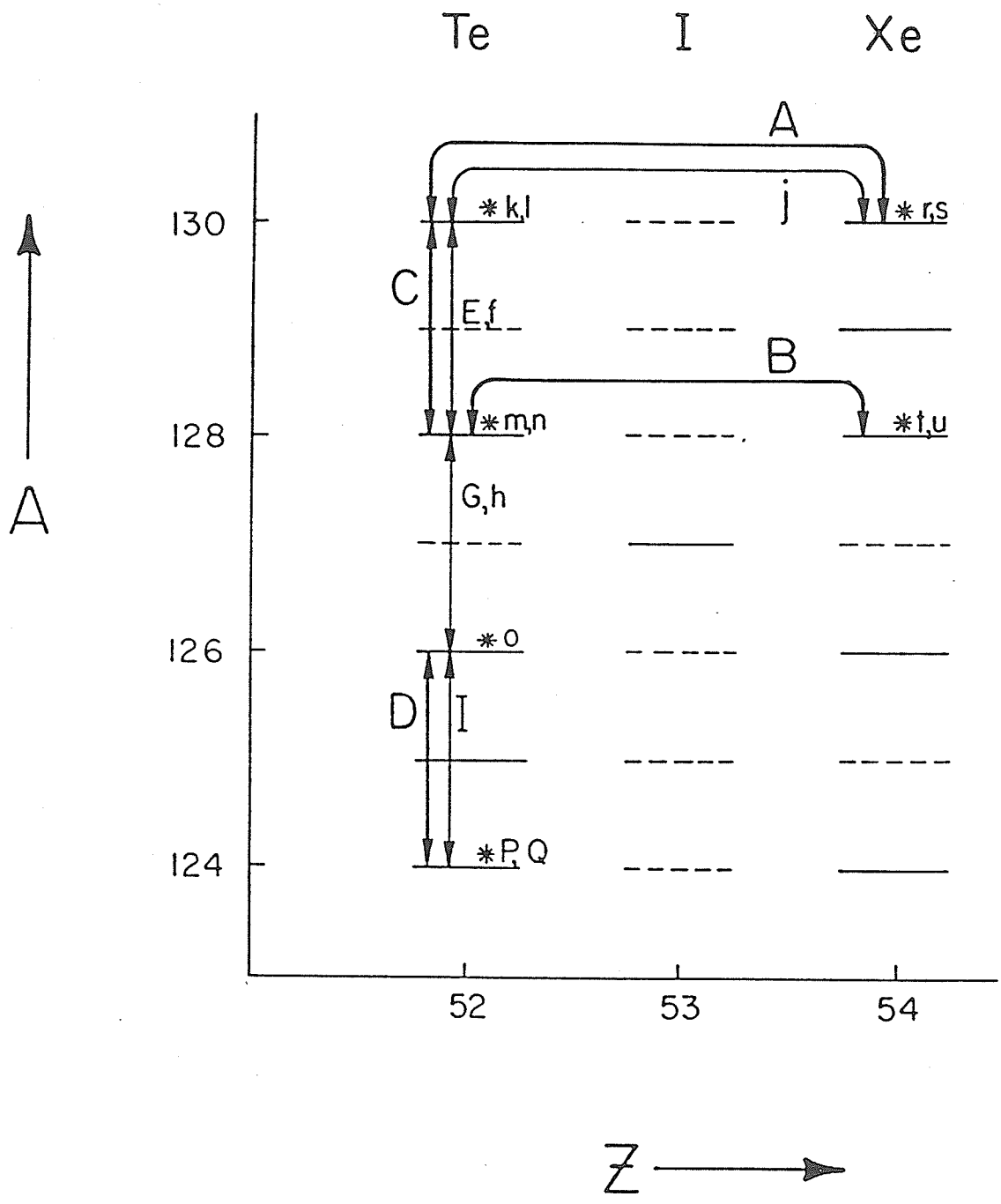

Figure 3.12 Schematic diagram of the Xe - Te input data. From [Dy 89]

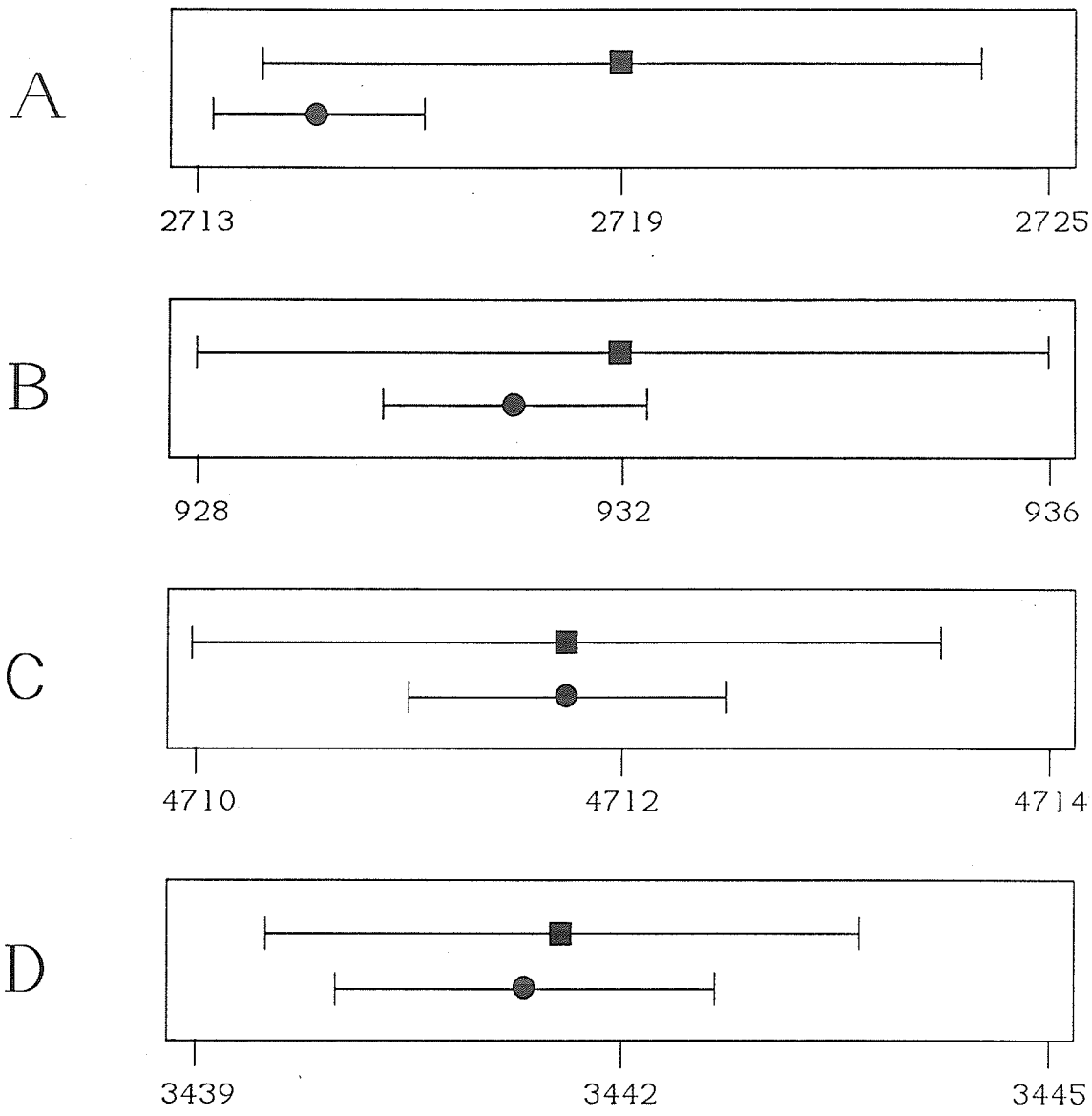

Figure 3.13 Comparison of the results of output values the Xe - Te adjustment (table 3.7) for the doublets measured in this work (table 3.5) with the 1983 Mass Evaluation [Wa 85].
Circles represent the values from this work and squares represent the values from the 1983 Mass Evaluation.

3.5 Tables for Chapter 3

Instrument	B_{11}	B_{12}	B_{22}	B_{33}
Manitoba I	0.9341	0.1974	-0.8294	-17.23
Manitoba II	0.09627	0.3103	1.296	12.17
Minnesota	0.1041	-0.1772	1.356	27.63
Harvard	0.2486	6.134	1.393	15.49
Mainz	0.0754	-12.08	-10.03	-478.0
Osaka I	5.473	-13.14	5.728	-26.58

Table 3.1 Second Order Image Aberration Coefficients from [Ma 71].

Code	Doublet	ΔM (this work)	Comparison value
A	$^{160}Gd^{35}Cl_2$ - $^{156}Gd^{37}Cl_2$	10 831.70 ± 1.27	10 831.05 ±1.21
B	$^{160}Gd^{35}Cl$ - $^{158}Gd^{37}Cl$	5 899.88 ± 0.96	5 899.90 ±1.08
C	$^{158}Gd^{35}Cl$ - $^{156}Gd^{37}Cl$	4 930.13 ± 1.36	4 931.15 ±0.55
D	$^{159}Tb^{35}Cl$ - $^{157}Gd^{37}Cl$	4 337.01 ± 0.61	4 336.89 ±1.19
E	$^{157}Gd^{35}Cl$ - $^{155}Gd^{37}Cl$	4 288.83 ± 0.66	4 288.21 ±0.55
F	$^{159}Tb^{35}Cl_2$ - $^{155}Gd^{37}Cl_2$	8 625.64 ± 1.03	8 625.10 ±1.31

Table 3.2 New mass spectroscopic doublet spacings (μu) in the Gd - Tb region. Comparison values are from the 1983 Atomic Mass Evaluation [Wa 85]

^{37}Cl	36.965 902 619	(112) u
^{35}Cl	34.968 852 728	(069) u
^{37}Cl-^{35}Cl	1.997 049 897	(110) u
^{37}Cl-^{35}Cl	2n-18 890.77	(10) keV
^{1}H	1.007 825 035	(012) u
^{2}H	2.014 101 779	(024) u
^{3}H	3.016 049 27	(04) u
^{13}C	13.003 354 826	(017) u
^{14}N	14.003 074 002	(026) u
^{54}Fe	53.939 612 7	(15) u
n	1.008 664 904	(014) u
e	548.580 26	(21) μu
1 keV	1.073 535 5	(30) μu

Table 3.3 Auxillary data for the least squares adjustments.

Code	Description	Input	Reference	Output
b_1	$Q_{EC}(^{157}Tb)$	64 ± 5	[1,2]	
		62.9 ± 0.7	[2,3,4]	
		62.92 ± 0.69[a]		63.04 ± 0.69
b_2	$Q_{EC}(^{158}Tb)$			1 220.64 ± 0.83
b_3	$Q_{B^-}(^{159}Tb)$	947 ± 7	[5,6,2]	971.61 ± 1.12
r_1	$Q(^{155}Gd(n,\gamma)^{156}Gd)$	8 536.0 ± 1.0	[7,8,2]	
		8 536.39 ± 0.12	[9]	
		8 536.38 ± 0.12[a]		8 536.32 ± 0.16
r_2	$Q(^{156}Gd(n,\gamma)^{157}Gd)$	6 359.8 ± 0.6	[8,10,2]	6 359.69 ± 0.37
r_3	$Q(^{157}Gd(n,\gamma)^{158}Gd)$	7 937.39 ± 0.12	[9]	
		7 937.1 ± 0.6	[11,8,2]	
		7 937.38 ± 0.12[a]		7 937.32 ± 0.16
r_4	$Q(^{158}Gd(n,\gamma)^{159}Gd)$	5 942 ± 1	[10]	5 941.94 ± 0.99
r_5	$Q(^{160}Gd(d,t)^{159}Gd)$	-1 200 ± 10	[12]	
	$Q(^{159}Gd(n,\gamma)^{160}Gd)$			7 453.01 ± 1.11
r_6	$Q(^{158}Tb(n,\gamma)^{159}Tb)$	8 160 ± 50	[13][b]	
		8 141 ± 39	[14][b]	
	$Q(^{159}Tb(d,t)^{158}Tb)$	-1 870 ± 15	[15]	
		8 131.3 ± 13.5[a]		8 134.20 ± 0.65
q_1	$Q(^{158}Tb(p,d)^{157}Tb) - Q(^{158}Gd(p,d)^{157}Gd)$	1 152.5 ± 4.0	[17][c]	1 157.60 ± 1.06
q_2	$Q(^{158}Gd(a,t)^{159}Tb) - Q(^{157}Gd(a,t)^{158}Tb)$	196.6 ± 1.0	[18]	
		198.3 ± 1.0	[16]	
	$Q(^{159}Tb(d,t)^{158}Tb) - Q(^{158}Gd(d,t)^{157}Tb)$	195.0 ± 1.5	[18]	
		197.00 ± 0.64[a]		196.87 ± 0.63
A	$^{160}Gd - ^{156}Gd$	4n - 27 691.78 ± 1.19		4n - 27 691.96 ± 0.76
B	$^{160}Gd - ^{158}Gd$	2n - 13 395.02 ± 0.90		2n - 13 394.95 ± 0.73
C	$^{158}Gd - ^{156}Gd$	2n - 14 298.35 ± 1.27		2n - 14 297.01 ± 0.40
D	$^{159}Tb - ^{157}Gd$	2n - 14 850.84 ± 0.58		2n - 14 850.88 ± 0.52
E	$^{157}Gd - ^{155}Gd$	2n - 14 895.72 ± 0.62		2n - 14 896.00 ± 0.38
F	$^{159}Tb - ^{155}Gd$	4n - 29 746.74 ± 0.97		4n - 29 746.89 ± 0.59

Table 3.4 Input data and results (keV) of the Gd - Tb adjustment.

a) Weighted mean.

b) Note: the original $Q_{\gamma,n}$ value is expressed as a $Q_{n,\gamma}$ value.

c) From the private communication in reference [17]; the published value (1 158.1 ± 4.0 keV) was in error.

References: 1 [Na 67], 2 [Wa 77], 3 [Be 83], 4 [Bh 62] 5, [Ma 58] 6 [Ni 58], 7 [Si 72], 8 [Bo 51], 9 [Is 82], 10 [Gr 71], 11 [Wh 73], 12 [Tj 67], 13 [Ch 58], 14 [Ge 60], 15 [Jo 70], 16 [Bu 75], 17 [Al 85], 18 [Bu 84]

Code	Doublet	^{4}M (this work)	Comparison value
A	^{130}Te - ^{130}Xe	2712.98 ± 2.84	2719 ± 5
B	^{128}Te - ^{128}Xe	931.26 ± 1.54	932 ± 4
C	$^{130}Te^{35}Cl$ - $^{128}Te^{37}Cl$	4711.57 ± 0.72	4711.7 ± 1.8
D	$^{126}Te^{35}Cl$ - $^{124}Te^{37}Cl$	3441.28 ± 1.54	3441.6 ± 2.1

Table 3.5 New mass spectroscopic doublet spacings (μu) in the Xe - Te region. Comparison values are from the 1983 Atomic Mass Evaluation [Wa 85]

Code	Description	^4M	Reference
E	$^{130}Te^{35}Cl$-$^{128}Te^{37}Cl$	4715 ± 2	[Ba 63]
f	$^{130}Te^{35}Cl$-$^{128}Te^{37}Cl$	4711.7 ± 1.8	[Ke 70]
G	$^{128}Te^{35}Cl$-$^{126}Te^{37}Cl$	4106 ± 2	[Ba 63]
h	$^{128}Te^{35}Cl$-$^{126}Te^{37}Cl$	4102.3 ± 1.8	[Ke 70]
I	$^{126}Te^{35}Cl$-$^{124}Te^{37}Cl$	3432 ± 2	[Ba 63]
j	^{130}Te-^{130}Xe	2706.2 ± 7.	[Ke 70]
k	C_9H_8N - ^{130}Te	159446 ± 10	[Da 63]
l	$^{13}CC_8NH_7$ - ^{130}Te	154990.6 ± 7.	[Ke 70]
m	$C_{10}H_8$ - ^{128}Te	158112 ± 9	[Da 63]
n	$C_{10}H_8$ - ^{128}Te	158141.2 ± 7.	[Ke 70]
o	$C_{10}H_6$ - ^{126}Te	143623 ± 9	[Da 63]
P	^{124}Te - $^{13}C^{37}Cl_3$	1754.6 ± 1.6	[Ha 84]
Q	^{124}Te - $^{54}Fe^{35}Cl_2$	25499.5 ± 2.7	[Ha 84]
r	$C_{10}H_{10}$ - ^{130}Xe	174743.6 ± 4.2	[Da 63]
s	$^{13}CC_8NH_7$ - ^{130}Xe	157695.4 ± 0.7	[Ke 70]
t	$C_{10}H_8$ - ^{128}Xe	159068.2 ± 4.2	[Da 63]
u	$C_{10}H_8$ - ^{128}Xe	159069.7 ± 0.7	[Ke 70]

Table 3.6 Previous mass spectroscopic data

CODE	DOUBLET	INPUT VALUES	OUTPUT VALUES	OUT-IN	CHISQ
1	^{130}Te	129906218.34 * 6.96	129906223.24 * 1.36	4.90	0.4955
2	^{128}Te	127904470.09 *14.15	127904461.62 * 1.26	-8.47	0.3585
3	^{126}Te	125903327.20 * 9.00	125903308.54 * 1.53	-18.66	4.2988
4	^{124}Te	123902817.35 * 1.40	123902817.35 * 1.25	0.00	0.0000
5	^{130}Xe	129903508.33 * 0.69	129903508.45 * 0.67	0.12	0.0324
6	^{128}Xe	127903530.62 * 0.70	127903530.58 * 0.67	-0.04	0.0041
7	^{130}Te-^{130}Xe	2712.98 * 2.63	2714.79 * 1.44	1.81	0.4711
8	^{128}Te-^{128}Xe	931.26 * 1.54	931.04 * 1.22	-0.22	0.0199
9	^{130}Te-^{128}Te	2001761.82 * 0.74	2001761.62 * 0.72	-0.20	0.0718
10	^{128}Te-^{126}Te	2001153.85 * 1.84	2001153.08 * 1.48	-0.77	0.1761
11	^{126}Te-^{124}Te	2000491.18 * 1.54	2000491.19 * 1.33	0.01	0.0000

Table 3.7 Input data and results (keV) of the Xe - Te adjustment.

Experiments at the Chalk River Nuclear Laboratories

4 Experiments at Chalk River Nuclear Laboratories

4.1 Equipment

4.1.1 The Chalk River On-Line Isotope Separator

The Chalk River on-line isotope separator (ISOL) [Sc 81] is illustrated in figure 4.1. It consists of a target-ion-source, followed by magnetic analyzer, a collection chamber, a beam transport line and a counting region. It can be operated on-line to either the MP tandem accelerator or the super-conducting cyclotron at the Chalk River TASCC (Tandem Accelerator Super-conducting Cyclotron) facility or off-line.

Two types of ion sources can be used with the ISOL: a helium jet ion source [Sc 87] and a FEBIAD ion source [Ki 76]. The helium jet ion source (see figure 4.2) utilizes a separate target chamber, at the end of a beam line, to produce the nuclides to be studied. Helium, loaded with sodium-chloride aerosols, is introduced into the target chamber at a pressure of approximately 1 atmosphere. Reaction products recoil out of the target and are thermalized within the target chamber by the helium and subsequently adhere to the aerosols. The gas, aerosols and reaction products are then transported by a 1mm diameter capillary to a skimmer. Here the mixture is blown out of the capillary towards a small skimmer orifice. The light helium gas diffuses over a large angle and only a small fraction passes through the orifice. The heavier aerosols, however, tend to travel straight through the skimmer hole and into the anode cylinder of the ion source. Here they are ionized by a plasma discharge and extracted from the source.

In the FEBIAD (for Forced Electron Beam Induced Arc Discharge) ion source the target is positioned immediately outside the ion source. Reaction products from the target pass through three carbon heat shields and a thin tantalum window and into a graphite catcher. The hot catcher then releases the products into the ion source plasma where they are ionized and extracted axially.

The original FEBIAD ion source design is illustrated in figure 4.3. In this source the cathode is heated by electron bombardment from a filament, which is mounted inside the cathode. An electron beam is extracted from the electron emitting surface of the cathode by a grid located a few millimeters away. A FEBIAD ion source has three possible operating modes: direct discharge mode, intermediate mode and oscillating electron discharge mode (the details are given by Kirchner and Roeckl [Ki 76]) which are selected by the choice of the outlet plate potential. The hole in the outlet plate acts as the object slit of the ion optical system and is, typically, 0.50 mm for mass measurements.

The magnetic analyzer is a 1.00m radius dipole magnet with a sector angle of 135° and a field index of n = 0.5. The distance between the ion source and the magnetic analyzer (l_m') is 1.00m and the distance from the exit of the magnetic analyzer to the focal plane is 1.64m. This configuration gives the analyzer a radial magnification of 1.25 and a dispersion of 2.25m. The magnetic analyzer also focuses in the vertical direction. The entrance boundary of the analyzer is concave with a radius of $R' = 0.35$ m, while the exit boundary is straight. This gives a focal plane that is tilted by 25° with respect to the beam axis.

The field in the median plane of a magnetic analyzer can be expressed as:

$$B(r) = B(r_0)\left[1 \; - \; \alpha\frac{r - r_0}{r_0} \; + \; \beta\left(\frac{r - r_0}{r_0}\right)^2 \; + \; \ldots \; \right]$$

where r_0 is the mean radius and $\alpha, \beta, \ldots$ are the field indices. The first index determines the slope of the plot of B vs r and the second index determines its curvature. The proper selection of these indices can give axial as well as radial focusing. Since the values of these indices may vary slightly with different settings of $B(r_0)$ the magnetic analyzer has a set of correction coils inside the pole gap that can be adjusted to tune the field indices. The analyzer has been designed with $\alpha \approx 0.5$ and $\beta \approx \alpha^2$.

The collection chamber (figure 4.1) contains beam diagnostic instruments, the image slit and an electrostatic deflector, which deflects the beam down a beam transport line.

The beam transport line (BTL) carries the beam from the collection chamber, through a shielding wall, to a low background area. It consists of a 20° electrostatic deflector and two electrostatic quadrupole doublets. The BTL can focus the beam to a spot a few millimeters in diameter between 0.5 and 0.7m from the last quadrupole.

The counting chamber is situated at the end of the BTL. It contains a Faraday cup, used in focusing the BTL, and a tape transport system. The tape transport system used in this experiment [Da 79] operates entirely within the vacuum system. A tape, from a standard data cassette, is located at the focus of the BTL. The beam is collected on it for a pre-determined period of time. The tape is then advanced so that the collected sample is moved away from the beam to a detector station where the decay spectrum from the collected sample is acquired.

The accelerating voltage is nominally 40 kV and its long term stability has been measured to be better than 1 ppm over six hours. The long term stability of the magnetic field has been shown to be 5 ppm or better under adverse conditions. The statistical fluctuations of values for the measurements are about 5 ppm about the mean, however, which suggests a field instability of no worse than 2.5 ppm, since this would contribute a 5 ppm uncertainty to the position of the centroid, for this experiment. The power supplies for the ion source are stabilized to 0.3% over eight hours, with less than 0.5% ripple. The extracted beam from the FEBIAD ion source has been measured to have an energy within two volts of the full extraction voltage. In off-line measurements resolving powers of R = 20 000 have been achieved; typical resolving powers for on-line measurements are 5 000 to 6 000 [Sh 89].

4.1.2 Data Acquisition

A block diagram of the mass measurement system is given in figure 4.4. As in the measurements at the University of Manitoba, a peak matching technique is employed, but here the peaks are generated not by the direct detection of the ions themselves, but by the detection of their radioactive decay signatures. The technique is, thus, unaffected by unresolvable beams from isobars or even isomers, provided they have distinguishable decay signatures.

Small voltage steps are generated by the DAC and added to the accelerating voltage to sweep the beams from each nuclide across the image slit. The deflector and all of the electrostatic elements in the BTL are swept to follow the accelerating voltage in accordance with the Swann-Bleakney theorem (see section 3.1.1.2). At each voltage a sample is collected on the tape and then moved to a detector, which

records the decay spectrum. The time sequence of a measurement is illustrated in figure 4.5. At the beginning of a cycle the separator beam is deflected (a) so that no beam is accumulated on the tape and the accelerating voltage and the voltages on all of the electrostatic elements are adjusted and allowed to settle (b). Then the beam deflector is turned off and a sample is collected on the tape (c) while the accelerating voltage is measured (d). Before this cycle begins again, the tape is moved (e) to the counting station during the time that the beam is deflected. Here the gamma-ray spectrum is recorded (f), while the next sample is being collected. At the end of the spectrum measurement the data are transferred to magnetic tape.

At the end of each voltage point areas under the gamma-ray peaks which are characteristic of the decay of the nuclide being measured are integrated by the computer. A mass peak can then be generated by plotting these gamma-ray areas versus the measured voltage. Figures 4.10 through 4.12 are examples of this type of plot and show the integrated areas in the upper half and the corresponding, added voltage in the lower half. Currently, the voltage is not swept across the peaks one after the other, but is switched back and forth between the two masses from the center of each peak towards the edges, to minimize the effects of any drifts. As well as mass doublets, triplets can be measured, in which three different masses are scanned simultaneously, as shown in figure 4.12

During the acquisition, the data are roughly analyzed, on-line, and displayed to allow the experiment to be monitored and any necessary parameters to be tuned. Computer programs are later used, off-line, to generate the peaks, evaluate their centroids, with respect to voltage, and determine the corresponding mass difference. Since the complete gamma-ray spectrum has been stored for each voltage, the data

can be re-analyzed to provide mass measurements of any isobaric activity found in the spectra, after determining that the activity was produced directly and not from the decay of the isobaric parent nuclide.

4.2 Indium Mass Measurements

4.2.1 Motivation

A knowledge of the masses of the light isotopes of indium is important for several reasons. It provides mass measurements far from the valley of beta stability, which are currently of great interest (see section 2.6). It also gives information about the shape of a portion of the mass surface near the doubly magic nuclide ^{100}Sn and the strength of the expected shell closure at N = Z = 50.

A recent measurement of the masses of $^{103\text{-}105}$In by Wouters et al. [Wo 83] (the first time that the masses of these isotopes had been measured) indicated that two of these isotopes were more tightly bound, by as much as 1 MeV, than was expected from the systematics of the region. The degree of this discrepancy can be seen in the S_{2n} values plotted in figure 4.6. This anomalously large binding energy would suggest a huge departure from the expected trends in nuclear binding in this region, perhaps due to its proximity to ^{100}Sn, as ^{103}In and ^{97}Pd are the nuclides closest to ^{100}Sn whose masses have been measured.

The measured values of the In masses also deviate strongly from the masses predicted by the mass formulae. The shell model type of calculations predict the masses of the other isotopes of In (from A = 106 to A = 131) fairly well, in general, and many of the liquid drop model calculations, though they are less accurate for the higher mass indium isotopes, agree with the predictions of the shell model calculations

for the masses of $^{103\text{-}105}$In. These formulae predict that ^{103}In, for example, should be less tightly bound than indicated by the measurement of Wouters et al. by, again, about 1 MeV.

After the publication by Wouters et al. precise Q_{EC} measurements for ^{105}In were made by Verplancke et al. (Q_{EC} = 4 840 ± 130 keV [Ve 84]) and Bom et al. (Q_{EC} = 4 850 ± 13 keV [Bo 86]). Bom et al. later made similar Q_{EC} measurements of ^{103}In and ^{104}In (Q_{EC} = 6 050 ± 20 keV and Q_{EC} = 7 800 ± 250 keV, respectively [Bo 88]). While the precisions of the ^{105}In and ^{103}In measurements are much higher than could be obtained by a direct mass measurement, yielding masses of 104 914 661.3 ± 17.5 μu and 102 919 906.9 ± 27.2 μu respectively, the precision of the ^{104}In measurement is somewhat poorer. The ^{104}In Q_{EC} measurement was also complicated by: (a) the presence of ^{104}Ag and ^{104m}Ag, necessitating a difficult separation of the components; (b) the lack of an adequate level scheme to describe the ^{104}In β spectrum, necessitating the use of mean decay energies; (c) an unexpectedly high beta intensity in the low energy region spectrum, indicating strong feeding to the high energy levels in Cd. Because these complications were present, it was necessary to estimate the size of the potential systematic errors. Accordingly, direct measurement of the mass of ^{104}In was important, not only to tie down this contentious mass, but also to check the previous measurement for any gross errors.

4.2.2 Experimental Details

In an effort to resolve this large discrepancy, we have used the Chalk River ISOL to measure the mass differences between ^{103}In, ^{104}In and ^{105}In. Although an attempt was made to make the measurement in January 1988 with the Helium Jet ion

source, low yields and the instability of the ion source precluded any conclusive results. The measurement was later made in October 1988 with the FEBIAD ion source.

The desired indium isotopes were produced by the appropriate ^{92}Mo(^{16}O,pxn) reaction. For the ^{105}In - ^{104}In mass difference measurements, a 92 MeV beam of $^{16}O^{6+}$ with a current of approximately 800 nA was used on a target of enriched ^{92}Mo. For the measurement of the ^{104}In - ^{103}In mass difference and for the ^{105}In - ^{104}In - ^{103}In mass triplet measurements a 110 MeV beam of $^{16}O^{7+}$ at currents of approximately 1 μA and 2.4 μA, respectively, were used on the same target material. All targets were 2 mg/cm^2 thick.

Gates were set on gamma-ray peaks at 187.91 keV for ^{103}In, 658.0 keV and 834.1 keV for ^{104}In and 137.47 keV and 260.27 keV for ^{105}In Typical gamma ray spectra of samples collected at masses 103, 104 and 105 are shown in figures 4.7, 4.8 and 4.9 respectively.

4.2.3 Results

Nineteen mass measurement runs were made. Fifteen of these were measurements of the ^{105}In - ^{104}In mass difference, two were of the ^{104}In - ^{103}In mass difference and two were mass triplets. Many of the runs consisted of more than one scan. Each scan was carefully examined and any which contained unreliable voltage measurements (due to ion source sparking, for example) which were made within the mass peak portions of the scan were rejected. Scans which had bad voltage measurements in the background areas of the scan had the incorrect voltage replaced with an extrapolated voltage, so that they could be analyzed. After this filtering

procedure nineteen good scans remained from the original twenty-five. Typical examples of the mass and voltage spectra for each of the three types of measurement are given in figures 4.10, 4.11 and 4.12.

The precise values of Bom et al. for the masses of ^{105}In and ^{103}In [Bo 86, Bo 88] allowed us to use both the ^{105}In - ^{104}In mass difference measurements and the ^{104}In - ^{103}In mass difference measurements to derive a value for the mass of ^{104}In. The values for the mass of 104In derived from each mass scan are listed in table 4.1 and illustrated in figure 4.13. A weighted average of all of the data gives a value of 103 918 354. $\pm$ 73μu, with a χ^2 of 4.06. Thus, a final value, representative of the χ^2 inflated error, would be 103.918 35 (15) u.

The S_{2n} values which result from our measurements and those of Bom et al. are plotted in figure 4.6 along with those of Wouters et al. The new values lead to systematic trends in S_{2n} which are identical to the predicted systematic trends [Wa 83]. Separate plots of the S_{2n} values for even-N and odd-N nuclides better illustrates the underlying systematic trends in the region [Sh 77], as in figure 4.14. Here, the S_{2n} curves for indium are seen to be parallel to near by curves and the odd-n curve reproduces the slight downward break at N = 59. These systematics are similar to those observed in the region $92 < N < 126$, by Sharma et al. (see the discussion on page 1374 et seq. [Sh 77]). These measurements preclude the possibility of any large, unexpected deviations from the predicted trends in the nuclear binding energy of these near neighbors of the doubly magic ^{100}Sn.

4.3 Figures for Chapter 4

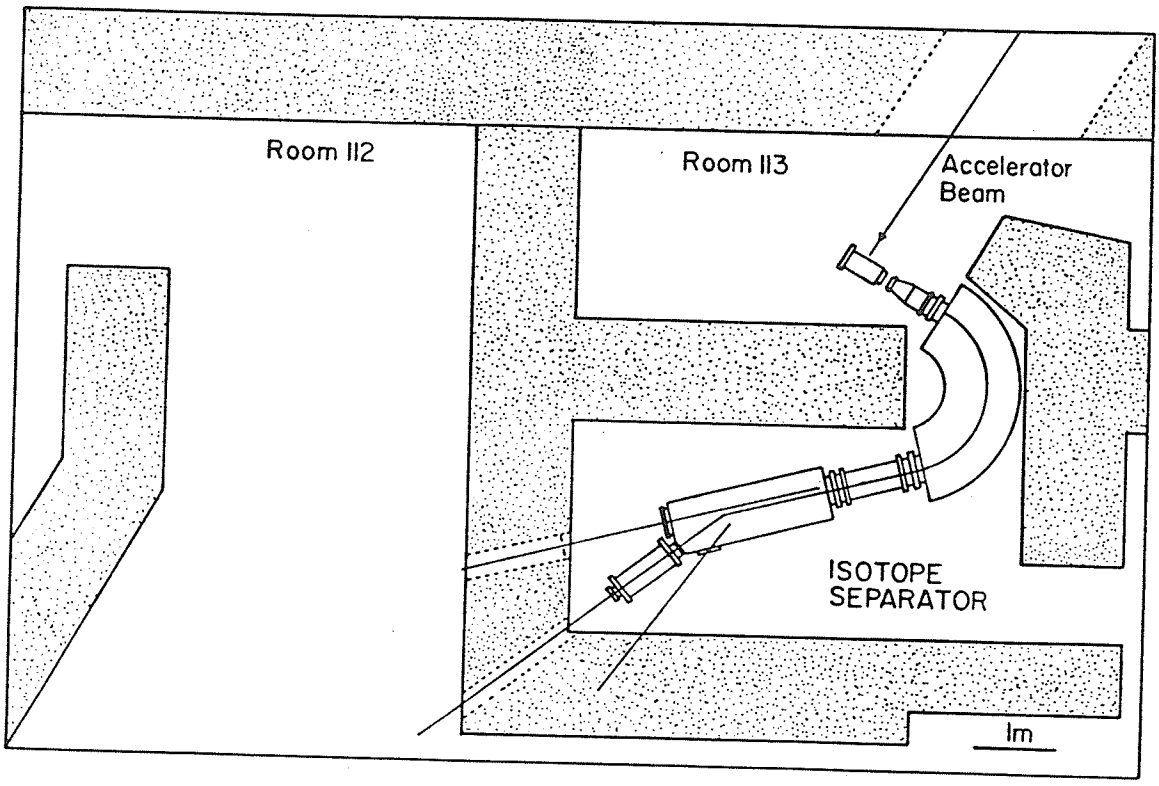

Figure 4.1 The Chalk River On Line Isotope Separator

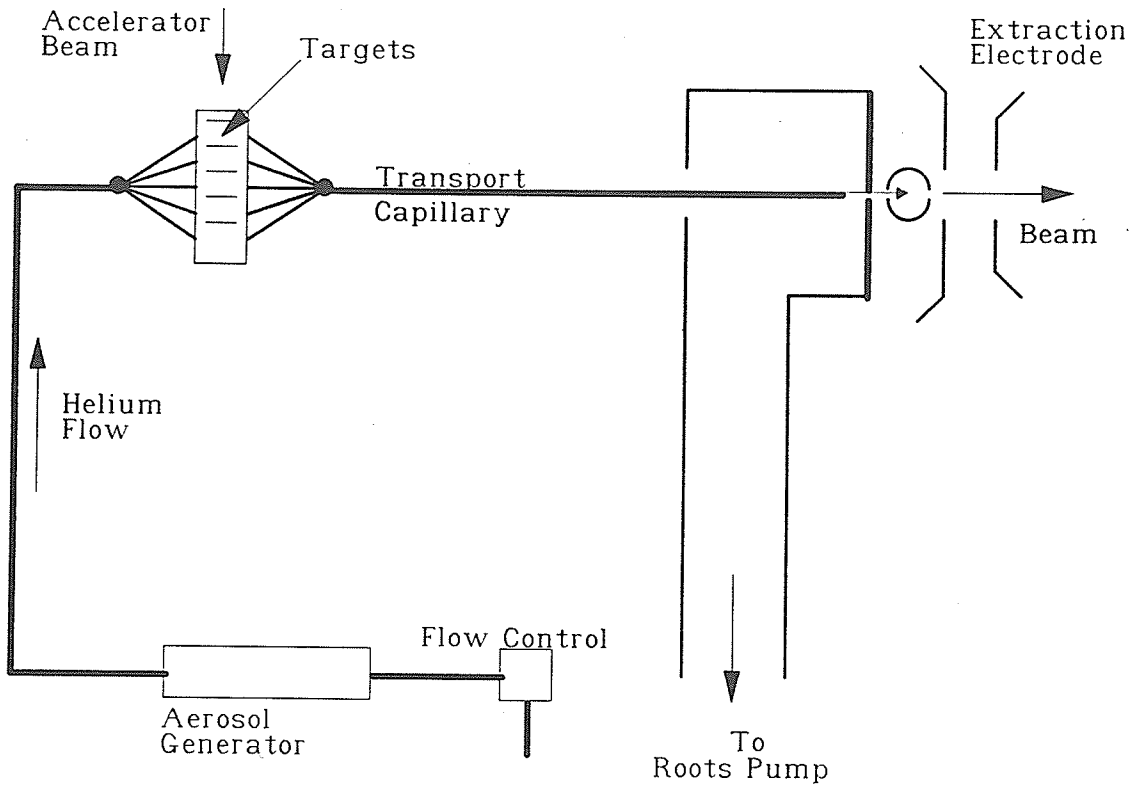

Figure 4.2 The Helium Jet ion source

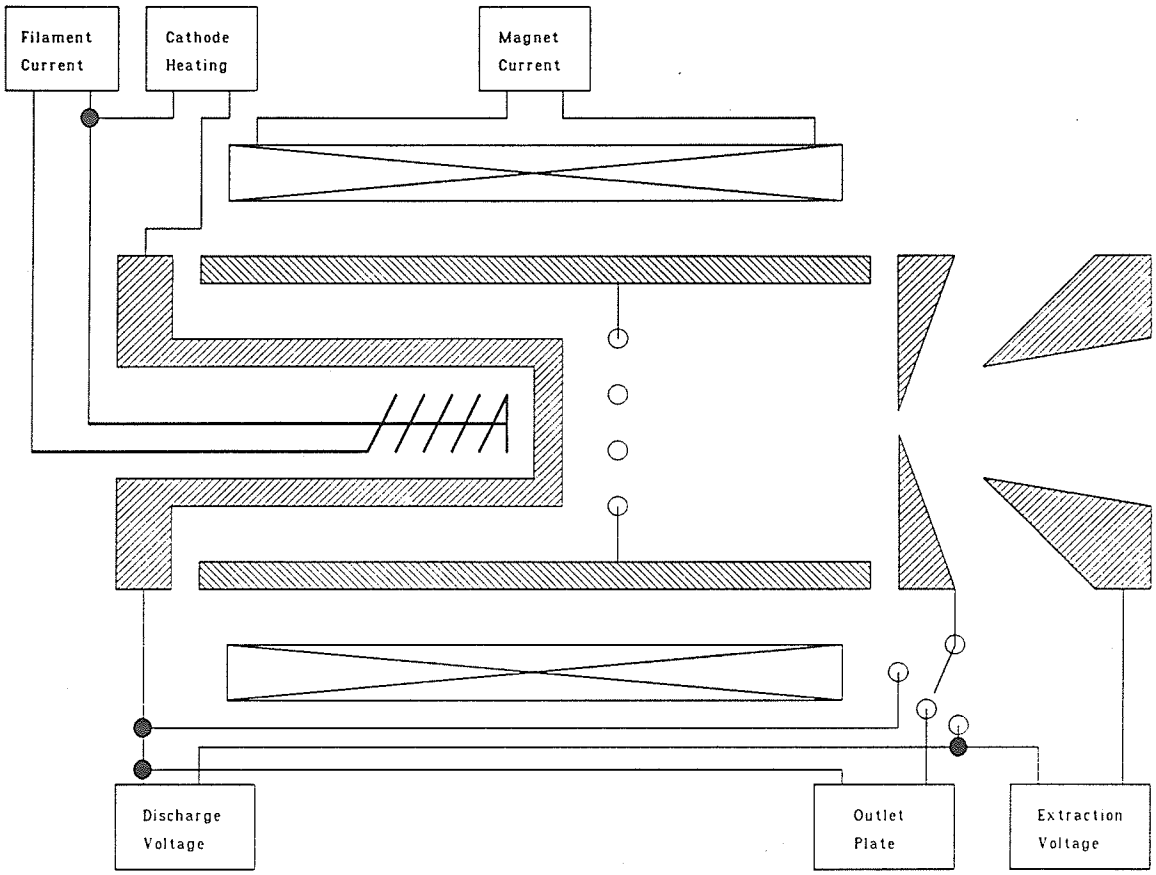

Figure 4.3 The FEBIAD ion source

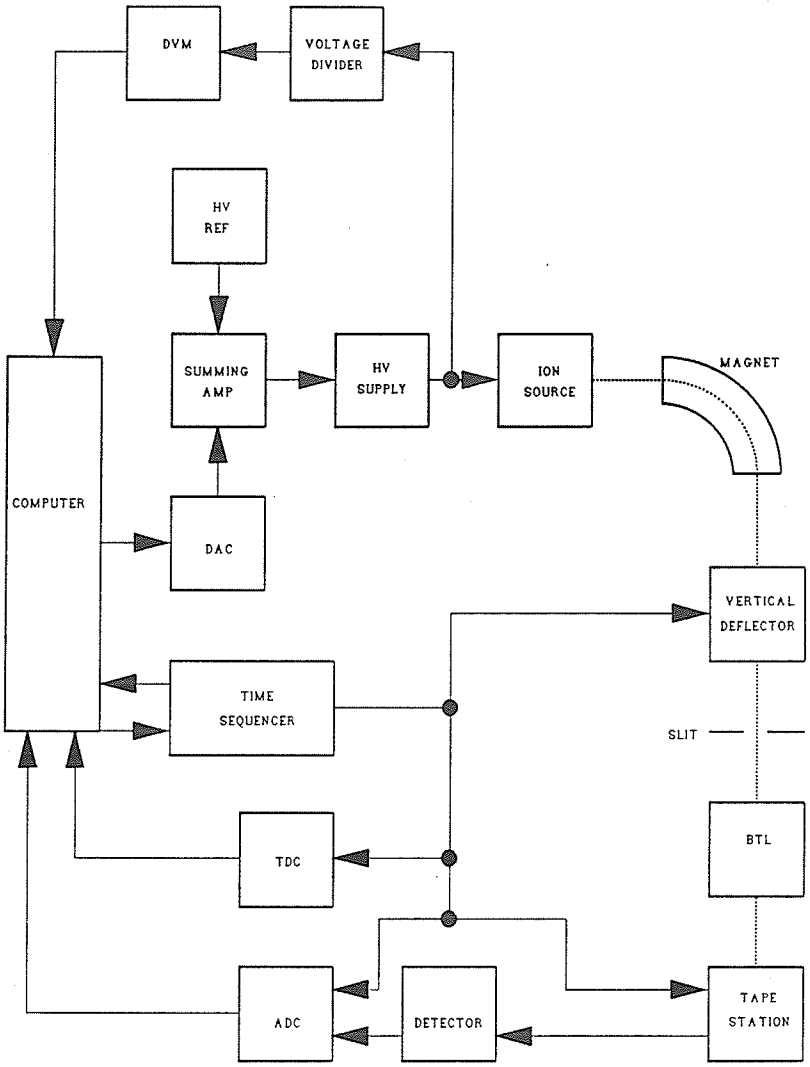

Figure 4.4 The Mass Measurement System
After Sharma et al. [Sh 89]

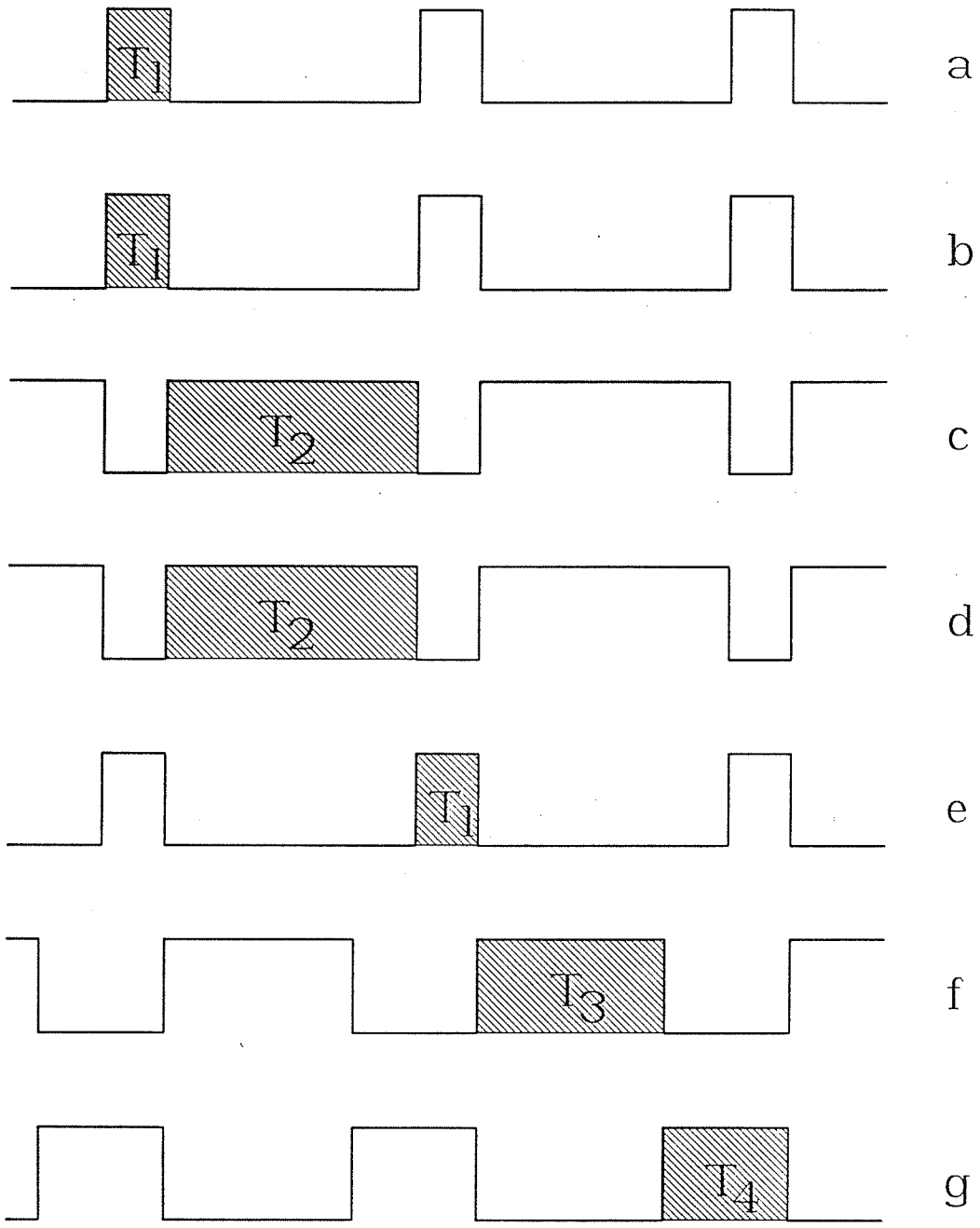

Figure 4.5 Timing Diagram for Mass Measurements
After Sharma et al. [Sh 89]

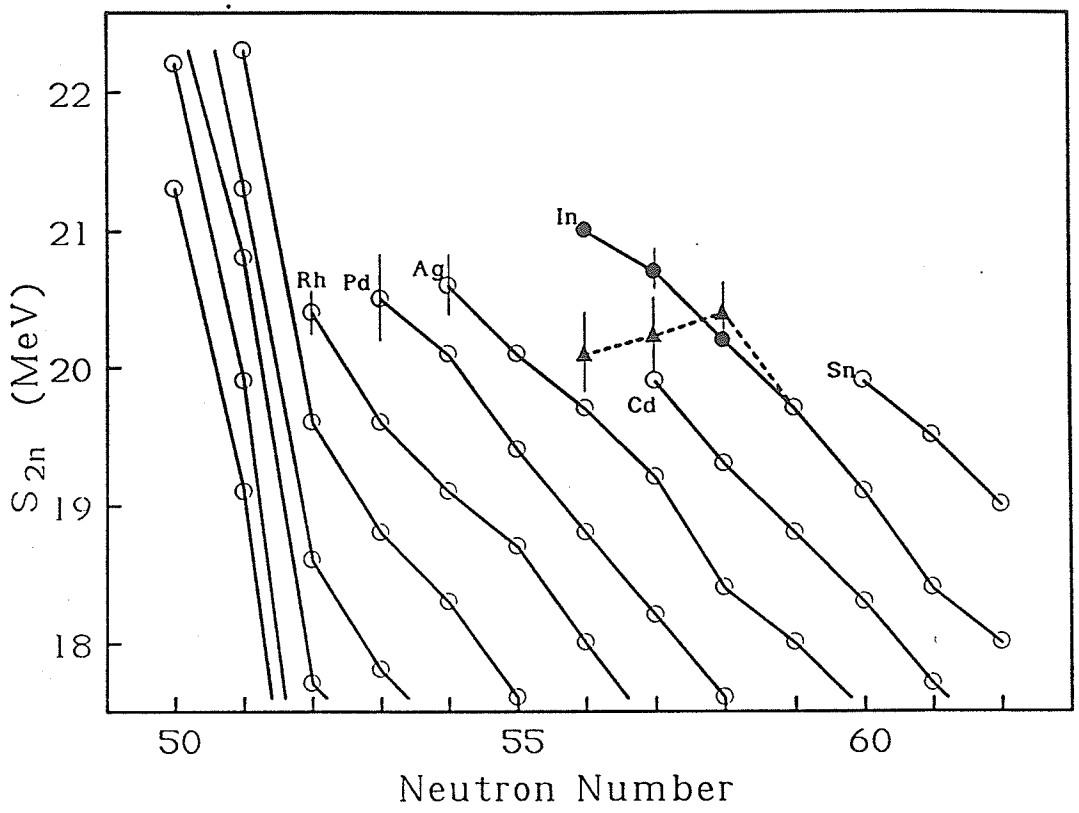

Figure 4.6 S_{2n} Values in the Vicinity of Z = 49
Solid triangles represent the measurements of Wouters et al. [Wo 83].
Solid circles represent this work and the work of Bom et al..[Bo 86,88].

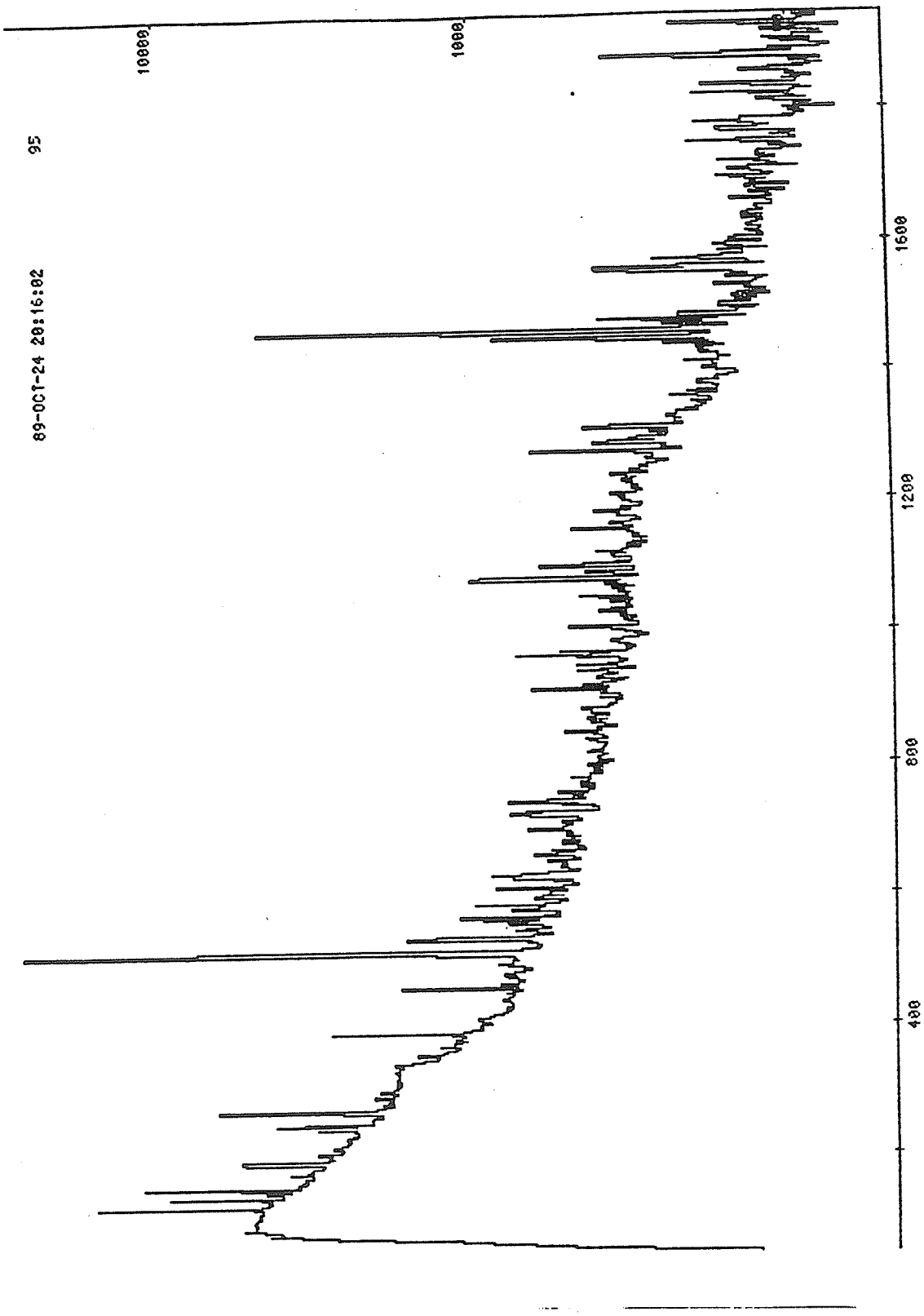

Figure 4.7 Gamma Ray Spectrum at Mass 103

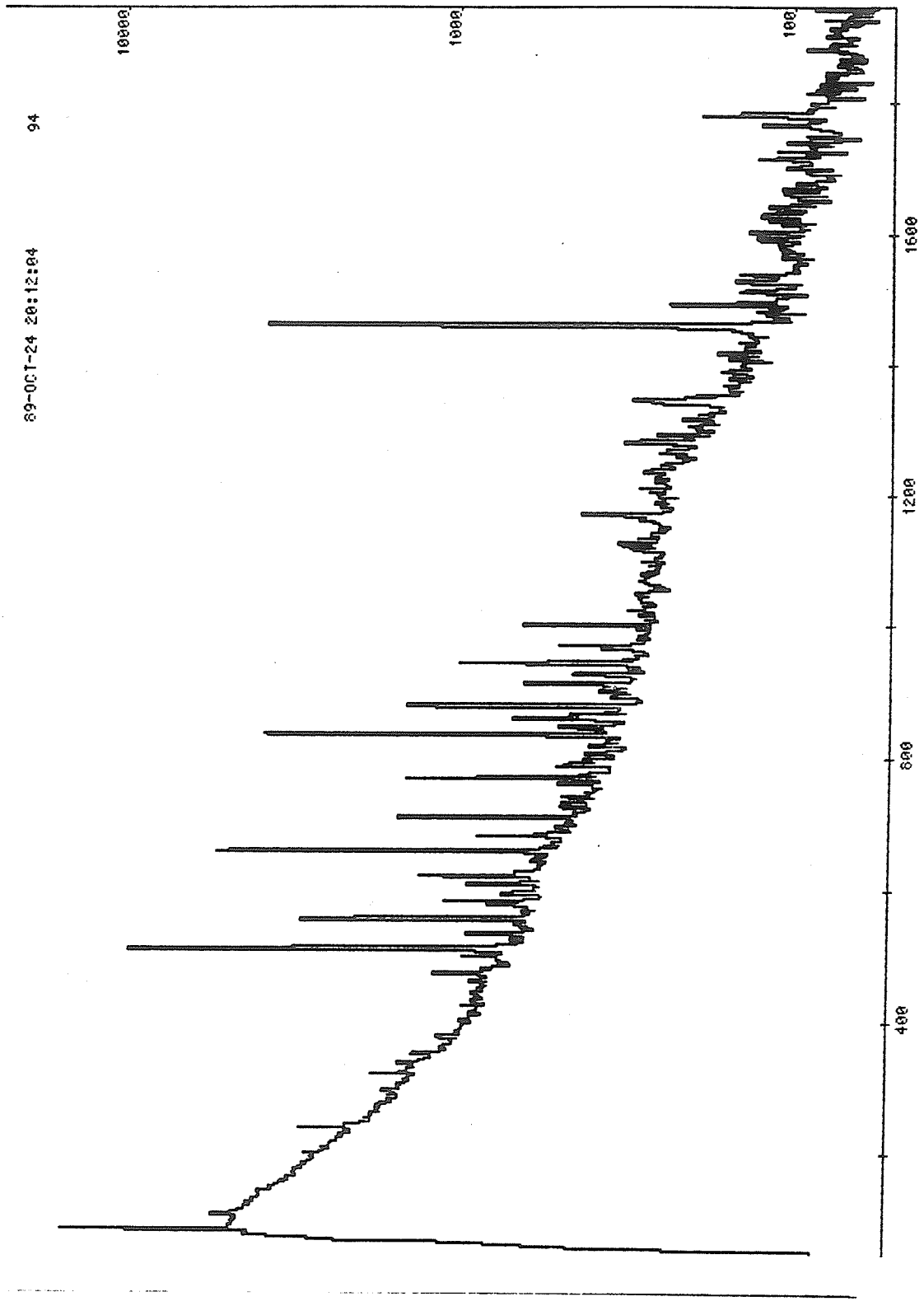

Figure 4.8 Gamma Ray Spectrum at Mass 104

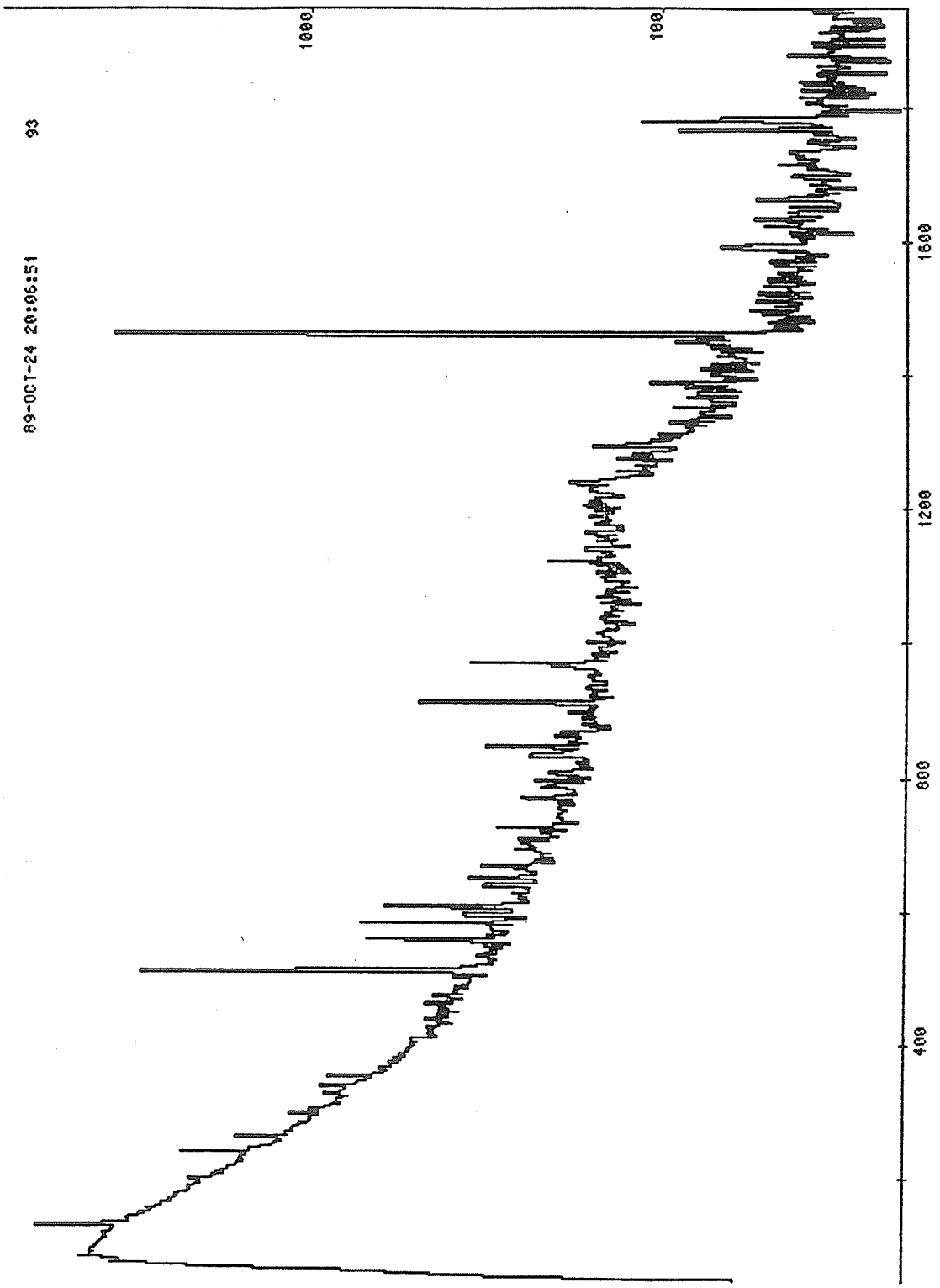

Figure 4.9 Gamma Ray Spectrum at Mass 105

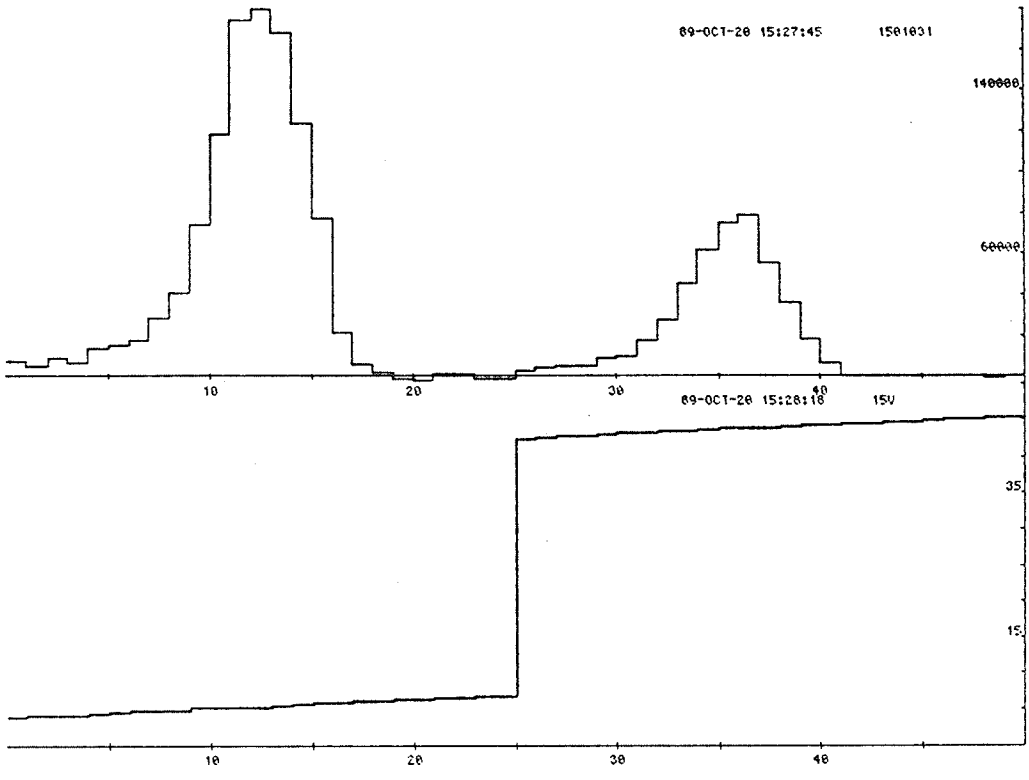

Figure 4.10 Mass and Voltage Spectra for ^{105}In-^{104}In Mass Measurement

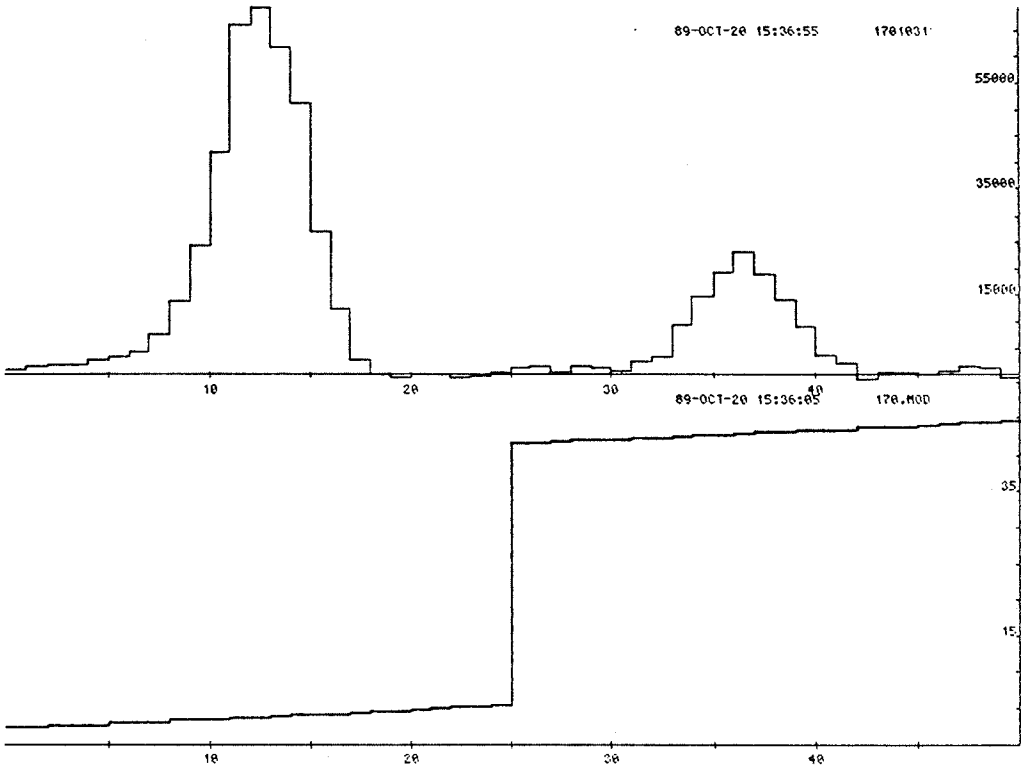

Figure 4.11 Mass and Voltage Spectra for ^{104}In-^{103}In Mass Measurement

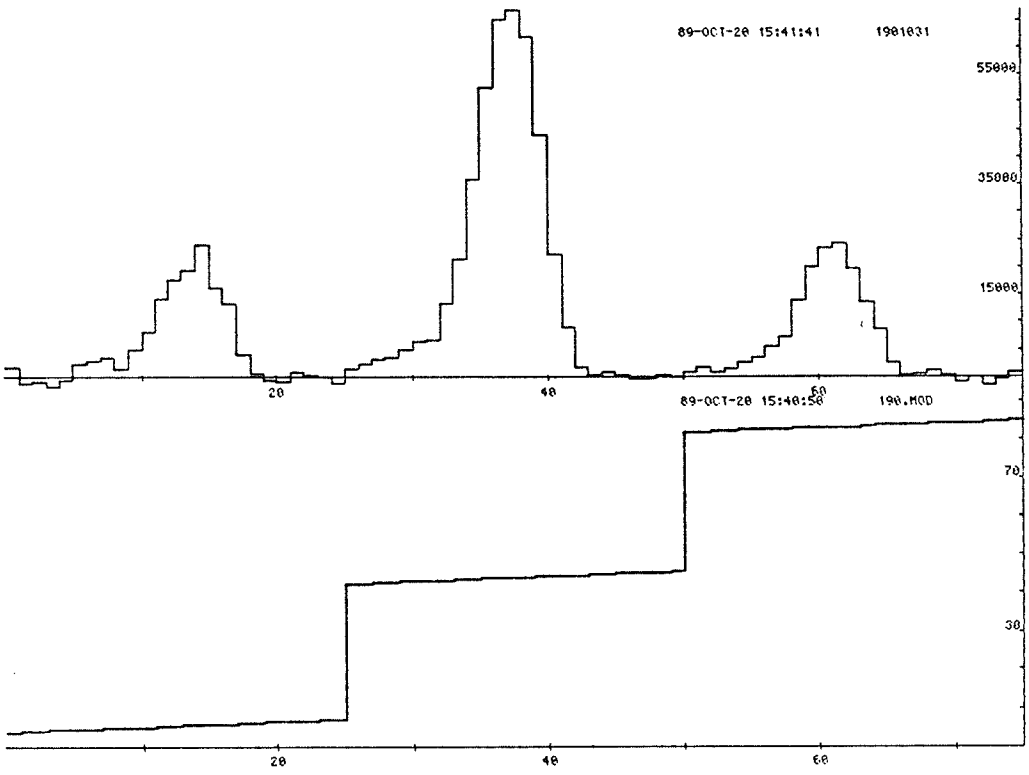

Figure 4.12 Mass and Voltage Spectra for ^{105}In-^{104}In-^{103}In Mass Triplet

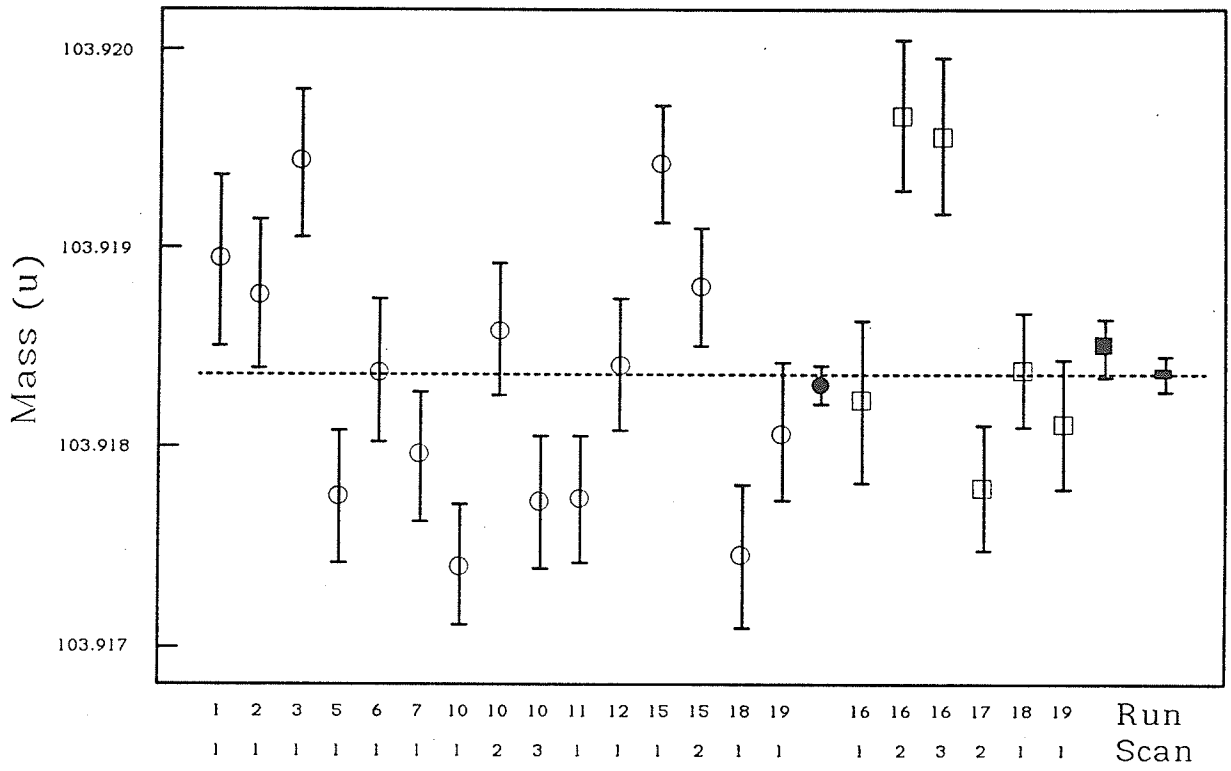

Figure 4.13 Scan by Scan Results of the ^{104}In Mass Measurements
Circles represent results from ^{105}In-^{104}In mass measurements.
Squares represent results from ^{104}In-^{103}In mass measurements.
Solid markers represent weighted averages
Dashes represent the final value.

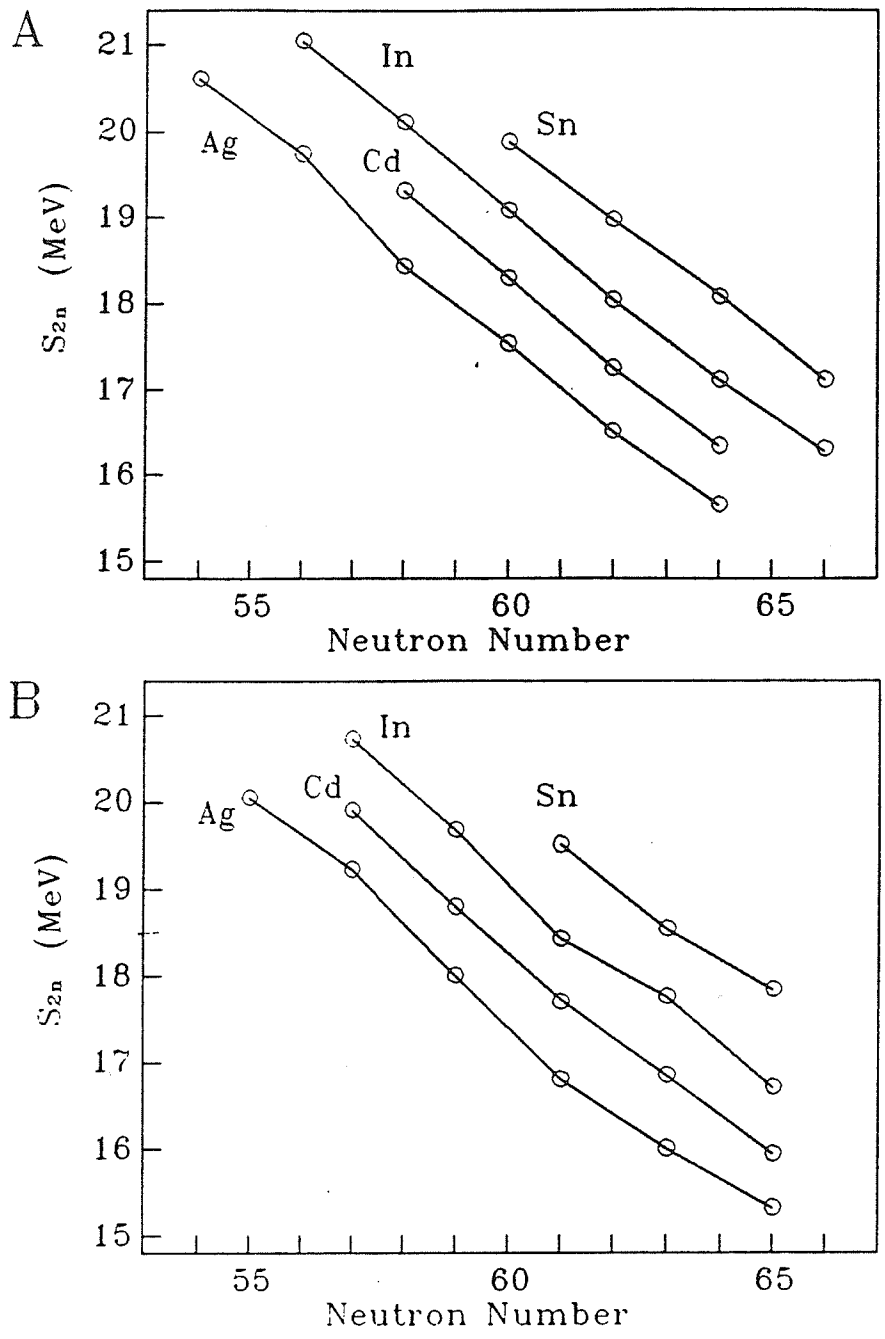

Figure 4.14 S_{2n} Values in the Vicinity of Z = 49
A S_{2n} Values of even-N nuclides
B S_{2n} Values of odd-N nuclides

4.4 Tables for Chapter 4

A

Run	Scan	M_{104}
1	1	103 918 937 ± 420 μu
2	1	103 918 759 ± 378 μu
3	1	103 919 430 ± 368 μu
5	1	103 917 741 ± 326 μu
6	1	103 918 371 ± 357 μu
7	1	103 917 951 ± 326 μu
10	1	103 917 395 ± 305 μu
10	2	103 918 581 ± 326 μu
10	3	103 917 710 ± 326 μu
11	1	103 917 720 ± 315 μu
12	1	103 918 402 ± 326 μu
15	1	103 919 420 ± 294 μu
15	2	103 918 801 ± 294 μu
18	1	103 917 447 ± 357 μu
19	1	103 918 066 ± 357 μu

B

Run	Scan	M_{104}
16	1	103 918 218 ± 410 μu
16	2	103 919 657 ± 378 μu
16	3	103 919 467 ± 399 μu
17	2	103 917 788 ± 315 μu
18	1	103 918 375 ± 294 μu
19	1	103 918 103 ± 325 μu

Table 4.1 Scan by scan results of the ^{104}In mass measurement
A) from ^{104}In - ^{105}In measurements
mean: 103 918 229.140 ± 86.193 μu; χ^2: 4.085.
B) from ^{104}In - ^{103}In measurements
mean: 103 918 502.257 ± 140.938 μu; χ^2: 4.499.

References

5 References

[Ab 67] W. Aberth and J.R. Peterson, The Review of Scientific Instruments. 38 (1967) 745.

[Al 85] T. Altzitzoglou et al., Physical Review C. 31 (1985) 360; M.M. Lowrey, private communication to K.S. Sharma (1985).

[Ar 62] M. von Ardenne, Tabellen Zur Angewandten Physik, Band 1 (veb Deutscher Verlag der Wissenschaften, Berlin) (1962).

[Av 83] F.T. Avignone III, H.S. Miley, R.L. Brodzinski and J.H. Reeves, Physical Review Letters. 50 (1983) 721.

[Av 88] F.T. Avignone III and R.L. Brodzinski, Progress in Particle and Nuclear Physics. 21 (1988) 99.

[Ba 63] R.C. Barber, W. McLatchie, R.L. Bishop. P. van Rookhuyzen and H.E. Duckworth, Can. J. Phys. 41 (1963) 1482.

[Ba 64] R.C. Barber, H.E. Duckworth, B.G. Hogg, J.D. Macdougall, W. McLatchie and P. Van Rookhuyzen, Physical Review Letters. 12 (1964) 597.

[Ba 71] R.C. Barber, R.L. Bishop, H.E. Duckworth, J.O. Meredith, F.C.G. Southon, P. van Rookhuyzen and P. Williams, Review of Scientific Instruments. 42 (1971) 1.

[Be 72] K.E. Bergkvist, Nuclear Physics. B39 (1972) 317.
K.E. Bergkvist, Nuclear Physics. B39 (1972) 371.

[Be 83] G.L. Beyer, A. De Rujula, R.-D. von Dincklage, H.A. Gustafsson, P.G. Hansen, H.L. Ravn and K. Riisager, Nuclear Physics. A408 (1983) 87.

[Bh 62] M.R. Bhat and M.L. Pool, Physical Reveiw. 127 (1962) 1704.

[Bi 63] R.L. Bishop, R.C. Barber, W. McLatchie, J.D. Macdougall, P. Van Rookhuyzen and H.E. Duckworth, Canadian Journal of Physics. 41 (1963) 1532.

[Bi 69] R.L. Bishop, PhD THESIS, Winnipeg: University of Manitoba Press (1969).

[Bi 70] R.L. Bishop and R.C. Barber, The Review of Scientific Instruments. 41 (1970) 327.

[Bl 36] W. Bleakney, Am. Phys. Teach. 4 (1936) 12.

[Bo 70] L.Ml Bollinger and G.E. Thomas, Physical Review C2 (1970) 1951.

[Bo 86] V.R. Bom, P.C. Coops, R.W. Hollander, E. Coenen, K. Deneffe, P. Van Duppen and M. Huyse, Zeitschrift fur Physik A. 325 (1986) 149.

[Bo 88] V.R. Bom, R.W. Hollander, E. Coenen, K. Deneffe, P. Van Duppen and M. Huyse, Zeitschrift fur Physik A. 331 (1988) 21.

[Bu 75] D.G. Burke and J.M. Balogh, Canadian Journal of Physics. 53 (1975) 948.

[Bu 84] D.G. Burke, Physical Review C. 29 (1984) 2339.

[Ch 58] B.G. Chidley, L. Katz and S. Kowalski, Canadian Journal of Physics. 36 (1958) 407.

[Co 65] L.E. Collins, R.H. Gobbett and P.T. Stroud, IEEE Transactions on Nuclear Science. NS-12, No.3 (1965) 247.

[Cu 49] S.C. Curran, J. Angus, A.L. Cockroft, Physical Review. 76 (1949) 853.

[Da 63] R.A. Damerow, R.R. Ries and W.H. Johnson, Jr., Physical Review. 132 (1963) 1673.

[Da 79] P. Dam, E. Hagberg and B. Jonson, Nuclear Instruments and Methods. 139 (1979) 427.

[De 38] A.J. Dempster, Physical Review. 53 (1938) 64 & 869.

[De 62] R.A. Demrikhenov, H. Ffolich, Report of the 1st International Conference on High Energy Accelerators. (1962) 224.

[Di 85] R.-D. von Dinklage, J. Gerl, H.L. Ravan and G.J. Beyer, Physical Review, C31 (1985) 1510.

[Do 81] M. Doi, T. Kotani, H. Nishiura, K. Okuda and E. Takasugi, Physics Letters. 103B (1981) 219.

[Du 54] H.E. Duckworth, Nature 174 (1954) 595.

[Du 86] H.E. Duckworth, R.C. Barber and V.S. Venkatasubramanian, Mass Spectroscopy, (1986) Cambridge: Cambridge University Press.

[Dy 85] G.R. Dyck, R.J. Ellis, K.S. Sharma, C.A. Lander, R.C. Barber and H.E. Duckworth, Physics Letters. 157B (1985) 139.

[Dy 89] G.R. Dyck, M.H. Sidky, J.G. Hykawy, C.A. Lander, K.S. Sharma, R.C. Barber and H.E. Duckworth, Physics Letters. Submitted for Publication.

[El 85] R.J. Ellis, R.C. Barber, G.R. Dyck, B.J. Hall, K.S. Sharma, C.A. Lander and H.E. Duckworth, Nuclear Physics. A435 (1985) 34.

[El 87] S.R. Elliot, A.A. Hahn and M.K. Moe, Physical Review C. 36 (1987) 2129.

[Ep 79] M. Epherre, G. Audi, C. Thibault, R. Klapisch, G. Huber, F. Touchard and H. Wollnik, Physical Review C. 19 (1979) 1504.

[Fe 34] E. Fermi, Z. Phys. 88 (1934) 161.

[Fi 82] G.B. Field, Mercury. 11, No.4 (1982) 74.

[Ge 60] K.N. Geller J. Halpern and E.G. Muirhead, Physical Review. 118 (1960) 1302.

[Ge 79] M. Gell-Mann, P. Ramond and S. Slansky, Supergravity, ed. P. van Nieuwenhuizen and D.Z. Freedman, (1979) Amsterdam: North-Holland.

[Gi 87] A. Gillibert, W. Mittig, L. Bianchi, A. Cunsolo, B. Fernandez, A. Foti, J. Gastebois, C. Gregoire, Y. Schutz and C. Stephan, Physics Letters. B192 (1987) 39.

[Gr 71] L.V. Groshev et al., Izv. Akad. Nauk Ser. Fiz. 35 (1971) 1644.

[Gr 83] K. Grotz, H.V. Klapdor and J. Metzinger, J. Phys. G: Nucl. Phys. 9 (1983) L169.

[Gr 86] K. Grotz and H.V. Klapdor, Il Nuovo Cimento. 9C (1986) 535.

[Ha 82] W.C. Haxton, G.J. Stephenson, Jr. and D. Strottman, Physical Review D. 25 (1982) 2360.

[Ha 84] B.J. Hall, R.J. Ellis, G.R. Dyck, C.A. Lander, R. Beach, K.S. Sharma, R.C. Barber and H.E. Duckworth, Physisc Letters. 138B (1984) 260.

[Hi 59] H. Hintenberger and L.A. König, Advances in Mass Spectrometry, Vol.1, ed. J.D. Waldron, (1959) New York: Pergamon Press, p. 16.

[Is 82] M.A. Islam, T.J. Kennett and W.V. Prestwich, Physical Review. C25 (1982) 3184.

[Jo 70] H.d. Jones and R.K. Sheline, Physical Review. C2 (1970) 1747.

[Ka 84] B. Kayser, Moriond Workshop on Massive Neutrinos in Astrophysics and in Particle Physics. 1984, 11.

[Ke 70] D.P. Kerr and K.T. Bainbridge, Recent Developments in Mass Spectrometry, ed. by K. Ogata and T. Hayakawa (University of Tokyo Press: Tokyo, 1970), p.490.

[Ki 65] J. Kistemaker, P.K. Rol and J. Politiek, Nuclear Instruments and Methods. 38 (1965) 1.

[Ki 76] R. Kirchner and E. Roeckl, Nuclear Instruments and Methods. 133 (1976) 187.

[Kl 85] H.V. Klapdor, Proceedings of teg VII International Summerschool on Nuclear Physics, Varna, Bulgaria (1985).

[Ko 47] E.J. Konopinski, Physical Review. 72 (1947) 518.

[Ko 79] K.S. Kozier, K.S. Sharma, R.C. Barber, J.W. Barnard, R.J. Ellis, V.P. Derenchuk and H.E. Duckworth, Canadian Journal of Physics. 57 (1979) 266.

[La 65] G.P. Lawrence, R.K. Beauchamp, and J.L. McKibben, Nuclear Instruments and Methods. 32 (1965) 357.

[Le 74] C. Lejeune, Nuclear Instruments and Methods. 116 (1974) 417.

[Le 89] M.A. Lee, Nuclear Data Sheets. 56 (1989) 199.

[Li 76] S. Liran and N. Zeldes, Atomic Data and Nuclear Data Tables. 17 (1976) 431.

[Ma 58] S.S. Malik, N. Nath and C.E. Mandeville, Physical Review. 112 (1958) 262.

[Me 71] J.O. Merideth, PhD THESIS, Winnipeg: University of Manitoba Press (1971).

[Me 72] J.O. Merideth and R.C. Barber, Canadian Jaurnal of Physics. 53 (1972) 1195.

[Mi 83] P. Minkowski, Nuclear Physics. B201 (1982) 269.

[Na 67] R.A. Naumann and P.K. Hopke, PhysicalReview. 160 (1967) 1035.

[Ni 58] K.O. Nielsen, O.B. Nielsen and O. Skilbreid, Nuclear Physics. 7 (1958) 561.

[Ov 80] D. Overbye, Sky and Telescope. 60, No.2 (1980) 115.

[Pa 33] W. Pauli, Handbuch der Physik, 24/1., Berlin: Springer-Verlag.
W. Pauli, Rapports du Septieme Conseil de Physique Solvay, Brussels, Paris: Gauthier-Villars et Cie. (1933).

[Po 68] B. Pontecorvo, Physics Letters. 26B (1968) 630.

[Pr 81] H. Primakoff and S.P. Rosen, Annual Review of Nuclear and Particle Science. 31 (1981) 145.

[Ra 83] R.S. Raghavan, Physical Review Letters. 51 (1983) 975.

[Ro 88] R.G.H. Robertson and D.A. Knapp, Los Alamos pre-print LA-UR-88-291, submitted to: Anual Review of Nuclear and Particle Science. (1988).

[Ru 81] A. de Rujula, Nuclear Physics. B188 (1981) 72.

[Sc 81] H. Schmeing, J.C. Hardy, E. Hagberg, W.L. Perry, J.S. Wills, J. Camplan and B. Rosenbaum, Nuclear Instruments and Methods. 186 (1981) 47.

[Sc 85] O. Scholten and Z.R. Yu, Physics Letters. 161B (1985) 13.

[Sc 87] H. Schmeing, J.S. Wills, J.C. Hardy, E. Hagberg, V.T. Koslowsky and W.L. Perry, Nuclear Instruments and Methods. B26 (1987) 321.

[Sh 74] A. de Shalit and H. Feshbach, Theoretical Nuclear Physics, Vol. 1. New York: John Wiley & Sons Inc. (1974).

[Sh 77] K.S. Sharma, J.O. Meredith, R.C. Barber, K.S. Kozier, S.S. Haque, J.W. Barnard, F.C.G. Southon, P. Williams and H.E. Duckworth, Canadian Journal of Physics. 55 (1977) 1360.

[Sh 86] D.P. Shelton, K.S. Sharma and R.C. Barber, Physics Letters. B176 (1986) 289.

[Sh 89] K.S. Sharma, H. Schmeing, H.C. Evans, E. Hagberg, J.C. Hardy and V.T. Koslowsky, Nuclear Instruments and Methods in Physics Research. A275 (1989) 123.

[Si 72] T.A. Siddiqi, F.P. Cranston and D.H. White, A179 (1972) 609.

[Si 78] G. Sidenius, Nuclear Instruments and Methods. 151 (1978) 349.

[Si 82] J. Silk, Nature 297 (1982) 102.

[So 77] F.C.G. Southon, J.O. Meredith, R.C. Barber and H.E. Duckworth, Canadian Journal of Physics. 55 (1977) 383.

[Sw 31] W.F.G. Swann, Journal of the Franklin Institute. 212 (1931) 439.

[Th 75] C. Thibault, R. Klapisch, C. Rigaud, A.M. Poskanzer, R. Prieels, L. Lessard and W. Reisdorf, Physical Review C. 12 (1975) 644.

[Tj 67] P.O. Tjom and B. Elbek, Kgl. Danske. Vid. Sel. Mat. Fys. Medd. 36 (1967) No.8.

[Tu 82] W. Tucker and K. Tucker, Mercury. 11, No.4 (1982) 81.

[Ve 84] J. Verplancke, E. Coenen, K. Cornelis, M. Huyse, G, Lhersonneau and P. Van Duppen, Zeitschrift fur Physik A. 315 (1984) 307.

[Vi 86] D.J. Vieira, J.M. Wouters, K. Vaziri, R.H. Kraus, H. Wollnik, G.W. Butler, F.K. Wohn and A.H. Wapstra, Physical Review Letters. 57 (1986) 3253.

[Wa 77] A.H. Wapstra and K. Bos, Atomic Data and Nuclear Data Tables. 20 (1977) 1.

[Wa 85] A.H. Wapstra and G. Audi, The 1983 atomic mass evaluation, Nuclear Physics. A432 (1985) 1.

[Wa 88] A.H. Wapstra, G. Audi and R. Hoekstra, Atomic Data and Nuclear Data Tables. 39 (1988) 281.

[Wh 73] D.H. White and T.A. Siddiqi, Nuclear Physics. A217 (1973) 410.

[Wi 80] F. Wilczek, Scientific American. 243, 6 (1980) 82.

[Wo 83] J.M. Wouters, H.M. Thierens, J. Aysto, M.D. Cable, P.E. Haustein, R.F. Parry and Joseph Cerny, Physical Review C. 27 (1983) 1745.

[Wu 57] C.S. Wu, E. Ambler, R.W. Hayward, D.D. Hoppes and R.P. Hudson, Physical Review. 105 (1957) 1413.

[Ze 80] A. Zee, Physics Letters B. 93 (1980) 389.